IEEE Access
Multidisciplinary | Rapid Review | Open Access Journal

Received July 24, 2019, accepted August 7, 2019, date of publication August 14, 2019, date of current version August 28, 2019.

Digital Object Identifier 10.1109/ACCESS.2019.2935307

Performance Analysis of Multi-Hop Broadcast Protocols for Distributed UAV Formation Control Applications

E. GIOVANNI CABRAL-PACHECO[1], SALVADOR VILLARREAL-REYES[1], (Member, IEEE), ALEJANDRO GALAVIZ-MOSQUEDA[1], SERGIO VILLARREAL-REYES[2], RAUL RIVERA-RODRIGUEZ[1], AND ALDO E. PEREZ-RAMOS[1]

[1]Center for Scientific Research and Higher Education at Ensenada (CICESE), Ensenada 22860, Mexico
[2]Monterrey Institute of Technology and Higher Education (ITESM), Monterrey 64849, Mexico

Corresponding author: Salvador Villarreal-Reyes (svillar@cicese.mx)

This work was supported in part by the Council for Science and Technology of Mexico (CONACYT) under Basic Scientific Research Grant 2016-01-285276.

ABSTRACT Multi-unmanned aerial vehicle (multi-UAV) systems have become popular in applications such as precision agriculture, remote sensing, and pollution monitoring. Commonly, multi-UAV systems require to reach and maintain a specific flight formation during mission execution. This can be achieved by using a distributed UAV formation control strategy in which each UAV has a flight controller whose function is to calculate the control actions for the UAV actuators such that the UAV formation is maintained. To perform this task, the control strategy requires the reliable and timely exchange of information within the UAV formation. The information that is needed by the controller is commonly referred to as state information (SI). It has been assumed that SI can be properly disseminated by means of multi-hop communications, i.e., by deploying a flying ad-hoc network (FANET). In this sense, multi-hop broadcast protocols (MBPs) that were previously proposed for mobile and vehicular ad-hoc networks seem to be suited for this task. However, previous work dealing with distributed UAV formation control has made communication and networking assumptions that would be hard to fulfill in actual FANET deployments. Moreover, the efficiency of the MBPs to disseminate SI within a FANET remains unexplored. The goal of this paper is to analyze how the network performance offered by different MBPs impacts the effectiveness of distributed UAV formation control to maintain UAV formation. An evaluation framework to perform this task is proposed in this paper. The simulation results demonstrate the relevance of MBP performance in SI message dissemination and thus in the ability of the controller to maintain a formation.

INDEX TERMS Broadcast, control, dissemination, multi-hop, FANET, UAV formation.

I. INTRODUCTION

Currently, the use of unmanned aerial vehicles (UAVs) has become very popular in both government (e.g., military) and civilian applications [1]–[4]. This popularity has gained momentum as a result of important technological advances in several areas, including embedded systems, energy storage, materials, sensors, and telecommunication systems, among others [5]. These advances have led to the development of small UAVs at affordable prices, which in turn have broadened the scope of the missions where multi-UAV systems can be used [6].

Using a group of small UAVs (e.g., a multi-UAV system) has many advantages regarding the cost, speed, scalability, and survivability of missions [7]. However, multi-UAV systems present different challenges that must be addressed for the successful deployment and execution of missions. For example, remote sensing multi-UAV missions can sweep large areas at once, but its execution requires that each UAV controls its position such that a spatial formation is achieved and maintained.

Multi-UAV missions strongly depend on wireless communications to exchange information [8]. The exchanged

The associate editor coordinating the review of this article and approving it for publication was Jiankang Zhang.

information can be of different types such as control commands, mission execution reports, and collected information that is downloaded from the UAVs to the ground station. Note that if direct UAV-to-ground (U2G) and ground-to-UAV (G2U) radio links are used to send control commands to the UAVs, then the mission range would be restricted to the radio coverage range [9]. Although private repeaters could be used to extend the radio coverage area, doing so may prove to be costly, impractical or both. Alternatively, satellite links could be used to extend the mission range, [10], but this would increase the mission cost and energy consumption.

Multi-UAV systems are often required to reach and maintain a specific flight formation (referred to as the UAV formation throughout the paper) during the mission execution [11]. In a UAV formation, a group of UAVs flies as a rigid entity, keeping the distances between individual pairs of UAVs fixed [12]. This procedure can be performed for different purposes. For example, by using a UAV formation in a remote sensing mission, more accurate or redundant sensed data could be acquired in a shorter period. Another advantage of flying in formation is that UAVs can keep a safe distance between each other so that potential collisions are avoided. Furthermore, by flying in formation, the mission coverage area can be increased in a coordinated way. Fig. 1 shows UAV formations that are commonly used in applications such as environment monitoring [13], precision agriculture [14], and aerial imaging [15]. These formations are commonly referred to as closed formations and can be used to sweep large monitoring areas or to reduce aerodynamic drag when UAVs move to the next mission area.

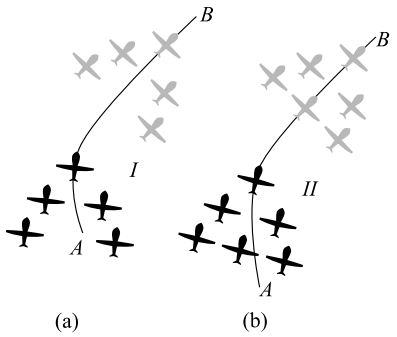

FIGURE 1. Typical UAV formations: (a) open-delta flight formation, and (b) delta flight formation. Open-delta formations are composed of external UAVs only, while delta formations are composed of external and internal UAVs.

Achieving and keeping a UAV formation is a challenging task, which requires each UAV to adjust its flight parameters (e.g., speed, orientation, and pitch) such that its relative position within the formation is maintained during the mission execution. Thus, each UAV must implement a formation controller (simply referred to as the controller in this work) whose task is to make the necessary control actions (e.g., speed, orientation, and pitch adjustments) to maintain its position within the formation. To be able to perform its task, the controller needs to have reliable and timely information about different kinematic variables during the mission execution, such as the relative position, speed, and attitude. The information that is needed by the controller to maintain the formation is commonly referred to as state information (SI), [16], and its content depends on the particular formation control strategy implemented.

In general, two different approaches are used for UAV formation control: centralized control and distributed control [17]. In centralized control, all computations and controls are performed in a ground station. Therefore, the use of U2G and G2U radio links is required to send each UAV the control actions to be performed, and then the mission coverage area will be limited by the transceivers radio ranges. In contrast, in distributed control schemes, all the calculations needed for the control actions are performed in each UAV [18]. Although U2G and G2U radio links could be used to send the required SI to each UAV, this would limit the mission coverage area. However, in addition to U2G and G2U links, UAV-to-UAV (U2U) radio links can be established within a UAV formation. These links can then be used to exchange information, thus defining a flying ad-hoc network (FANET), [7], [19]. FANETs are a subset of mobile ad-hoc networks (MANETs) in which the mobile nodes are UAVs. Therefore, UAVs can exchange information within a FANET without infrastructure support. Thus, when using a distributed approach for flight formation control, a natural approach would be to use a FANET for SI dissemination. This way, the mission coverage area is not necessarily limited by the U2G and G2U radio ranges. If the multi-UAV mission uses low-cost small UAVs with limited energy storage and radio resources, it might not be convenient to use a single hop approach for SI dissemination because of the power that is required by each transmission [6], [20], [21]. Instead, the use of multi-hop communications is attractive because of the possibility of using low-cost transceivers with reduced radio ranges and low power consumption. In this sense, the use of a multicast/broadcast protocol is a more efficient dissemination strategy compared to unicast routing protocols for the support of group communication applications [22]. Thus, the first natural approach to disseminate SI within a FANET would be to use multi-hop broadcast protocols (MBPs) that were previously proposed for MANETs or vehicular ad-hoc networks (VANETs). This paper analyzes the use of MBPs in FANETs for SI dissemination in distributed UAV formation control schemes and leaves the case of centralized control for a future contribution.

Disseminating information within FANETs is not a trivial task since FANETs present unique challenges regarding radio propagation, environmental conditions, mobility, and energy consumption [21], [23], [24]. For example, although in many cases there is line-of-sight between UAVs, fading may still occur because of ground reflections. Furthermore, factors such as variable packet delay, packet loss, and overhead are inherently present in ad-hoc networks. Thus, when using an MBP for SI dissemination, its network performance may adversely affect the performance of the distributed UAV

formation control strategy. For example, a decrease in the packet delivery ratio might affect the control strategy ability to keep UAV formation. Moreover, the MBPs that are commonly used for ad-hoc networks could perform differently under the network conditions that are found in FANETs. Therefore, there is a need to investigate if the use of different MBPs for SI dissemination within a FANET affects the performance of the distributed UAV formation control approach.

Several works addressing the design of distributed UAV formation control strategies consider that SI reaches the UAVs timely or within some fixed time window, [25]–[32]. For instance, [26] and [27] assume that this can be achieved by using enough transmission power to reach all UAVs within the formation with a single hop. In contrast, [28]–[31] consider using multi-hop communications to disseminate SI, whereas [32] assumes perfect communication between UAVs. However, all these works do not include the implementation or analysis of any particular multi-hop dissemination protocol. Furthermore, these contributions assume that the packet delay is constant while disseminating SI, which is not a realistic assumption when considering how multi-hop dissemination protocols work over ad-hoc networks (of which FANETs are a subset) [22]. Other works have considered the possible occurrence of impairments in the communications process, such as packet delays or packet drops, e.g., [33], [34]. For example, the authors in [33] consider that the communication process can experience time-varying delays and information losses. However, it is assumed that the blackout intervals do not exceed a known bound (1.3 s in the performed evaluations) and network connectivity can always be recovered. This means that if a UAV experiences a blackout period, it will be able to receive packets from its neighbors again once the blackout period has finished. However, actual transceivers have power constraints that limit their radio range. Therefore, if a UAV deviates enough from its intended position because of packet losses or a blackout, it may lose connectivity and get lost, regardless of the control strategy. Similarly, in [34], it is assumed that wireless connectivity is always available, and random packets delays are the only communication impairment. Furthermore, the results presented in [33] and [34] do not consider the implementation, performance, or analysis of actual multi-hop communication protocols. Thus, the assumptions that are made in these works would be hard to fulfill in actual FANET scenarios.

The goal of this paper is to analyze how the network performance offered by different MBPs impacts the effectiveness of distributed UAV formation control in maintaining the flight formation during the mission execution. In particular, this work evaluates the performance offered by Simple Flooding [35], Distance-Based [35], [36], Probability-based [37], and Counter-based [36] multi-hop broadcast strategies when they are used for SI dissemination in FANETs. Although these strategies are commonly used in MANETs and VANETs, to the best of our knowledge, their use for SI dissemination in FANETs has not been previously studied. To perform the evaluation, this paper introduces an evaluation framework (programmed in OMNeT++ and MATLAB®) to study the performance of multi-hop broadcast communications for SI dissemination in FANETs. Essential constraints on multi-UAVs deployments are considered in the framework, including maximum radio ranges for the wireless transceivers, UAV acceleration, UAV attitude, and propagation conditions. Different reference trajectory speeds and formation sizes can be defined within the evaluation framework. Thus, the framework provides a tool for studying how MBP performance affects the functioning of a distributed UAV formation control strategy. Without loss of generality, the model predictive control (MPC) scheme for distributed UAV formation control reported in [34] has been implemented in the evaluation framework. The use of MPC for distributed UAV formation control has been widely studied in the literature, e.g., [30]–[32], [34], [38], and [39]. Nevertheless, the analysis and results that are presented in this work can be used as a reference for the evaluation of other distributed UAV formation control strategies. Furthermore, the results and evaluation framework that are introduced in this work can be used to design and tune new distributed UAV formation control strategies.

The rest of the paper is structured as follows. Section II introduces the related work about distributed UAV formation control and MBPs. Section III introduces some background about the addressed problem, which is detailed in Section IV. Section V introduces the proposed evaluation methodology. The performance results and analysis are presented in Section VI. Finally, the concluding remarks and future work are provided in Section VII.

II. RELATED WORK

The goal of this paper is to analyze the suitability of several well-known MBPs when used in FANETs to disseminate the SI needed by distributed UAV formation control strategies. This section introduces related work addressing: multi-hop broadcast dissemination in FANETs; and distributed UAV formation control.

A. MULTI-HOP BROADCAST PROTOCOLS IN FANETs

FANETs can be considered to be a subgroup of VANETs, which are a subgroup of MANETs. Thus, it is natural to use protocols that were previously developed for MANETs and VANETs to address multi-hop broadcast dissemination within FANETs. In this sense, the use of MBPs within FANETs has been previously studied in [40]–[42]. In [40], fixed board-nodes were deployed at different predefined locations such that the physical distribution of the boards resembled typical UAV formations. By using this setup, three counter-based MBPs were evaluated for three different formation topologies. The results in [40] show that the performance of each protocol varies depending on the network topology. It is worth noting that, in this work, only the counter-based approach was considered. In addition, all the participating nodes were static during the evaluation. Thus, the impact of important factors such as the UAV speed was not

considered in the evaluation. Furthermore, the use of MBPs for SI dissemination was not addressed in [40]. The work done in [41] proposes the use of topological broadcasting in coordinated ground-flying ad-hoc networks to handle the issues related to the broadcast storm problem. In [41], UAVs are used as support nodes to keep ground nodes connected. For evaluation purposes, a simulation testbed based on NS-2 was proposed. UAVs were located at fixed waypoints over the area of interest to retransmit information between ground nodes. As in [40], the problem of SI dissemination for UAV formation control was not addressed in [41]. In [42], the performance of different information dissemination protocols that were originally designed for MANETs was compared for a simulated FANET scenario. Regarding the network conditions, the authors in [42] assume the free-space propagation model and no mobility for the UAVs in the simulation scenario. This means that, as in [40], the impact of important factors such as the UAV speed were not considered in the analysis provided in [42]. Thus, conclusions about the MBP performance for SI dissemination in flight formation control scenarios cannot be drawn from [42].

B. DISTRIBUTED UAV FORMATION CONTROL

As mentioned in the introduction, the evaluation framework uses a distributed UAV formation control strategy based on model predictive control (MPC), which has been widely studied in the literature, e.g. [30]–[32], [34], [38], and [39].

To the best of our knowledge, previous works dealing with the design of distributed UAV formation control strategies have not studied the impact of using actual MBPs to disseminate SI. For example, in early works proposing MPC for distributed UAV formation control such as [38], delays and packet losses related to communication impairments were not considered. In [39], the authors mention that fully decentralized MPC could use one-step previous information to address temporary communication failures. However, issues such as packet delays or burst losses were not considered. Furthermore, in [39], the authors only test the MPC with one leader and two one-hop wingmen, which does not require multi-hop communication. The problem of distributed UAV formation control is also addressed in [30]–[32]. Nevertheless, these works made assumptions related to the communication process, which would be difficult to fulfill in real-world FANET scenarios. For instance, the authors in [30] and [31] assume that every UAV must be connected to the leader through direct or multi-hop links. However, impairments that are commonly found in ad-hoc networking will cause disruptions in the communication flow; hence, this assumption is not always achievable. The authors in [32] assume that the communication between UAVs is perfect in terms of delay and losses, which is unrealistic in wireless communications. Although the analysis presented in [34] considers the possible occurrence of impairments in the communications process, the assumptions made do not reflect the actual behavior of information dissemination through ad-hoc networking. Particularly, it is assumed that wireless communication between UAVs is always available. Furthermore, it is considered that the only impairment caused by the communication process are random SI packet delays that are bounded. These assumptions would be hard to fulfill in actual FANET deployments because of the transceivers radio range, packet burst losses and similar issues arising in ad-hoc networking.

In summary, even though SI dissemination using multi-hop communications is feasible, factors inherently present in the communication process through FANETs (e.g., limited radio ranges, packet delays, packet losses, packet burst losses, and overhead), have not necessarily been considered in the evaluation of distributed UAV formation control strategies.

III. BACKGROUND

Before presenting the analysis and evaluation performed in this paper, it is necessary to provide a brief background regarding the MBPs that are evaluated and the distributed UAV formation control strategy used in the evaluation. First, some basic information about the MPC-based strategy implemented in the evaluation framework is presented. Afterward, a brief review of the different dissemination approaches used by the evaluated MPBs is provided.

A. DISTRIBUTED UAV FORMATION CONTROL

There are different distributed UAV formation control approaches proposed in the literature, such as leader-follower [17], [43]–[45], virtual structure [45], and behavioral [46]. All of these strategies require the exchange of SI among the UAVs. In a leader-follower strategy, the leader UAV is programmed to fly on some predefined reference trajectory while the follower UAVs are required to keep their preset distances (e.g., lateral and longitudinal) from the leader to maintain the formation. Thus, in a leader-follower approach, [17], [44], SI originates from the leader, and it must reach every UAV within a specific timeframe to maintain the formation. Similarly, if the SI does not reach each UAV in the formation on time, the performance of the virtual structure control strategy might decrease.

As mentioned in the introduction, without loss of generality, the evaluation framework implements an MPC-based distributed UAV formation control similar to that reported in [34]. Nevertheless, the analysis and results presented in this work can be used as a reference for the evaluation of other control strategies, knowing that in general, any distributed UAV formation control strategy will require the SI to reach each UAV within a specific timeframe to maintain the formation. The MPC-based distributed UAV formation controller reported in [34] is a feedback controller in which a trajectory optimization problem is solved in each time step. It can handle the constraints and nonlinearities of UAVs dynamics in a very intuitive way. Prior to this control strategy description, the kinematic model of the UAVs implemented in the evaluation framework will be provided next.

1) UAV KINEMATIC MODEL

Based on how they generate lift, UAVs can be classified as fixed-wing or rotatory-wing. Each of these approaches has different flight capabilities and limitations to consider when planning a mission. Regardless of this, distributed UAV formation control involves the design of distributed control laws under imperfect or partial measurements, which have to deal with the flight dynamics of the particular UAVs used for the mission. Thus, without loss of generality, fixed-wing UAVs are considered for the analysis presented in this paper. In particular, the analysis considers the two-dimensional motion of a fixed-wing UAV in a horizontal plane where each UAV is equipped with velocity hold and heading hold autopilots, as described in [47]. This assumption will enable to isolate UAV formation problems which can be directly related to the performance of the different MBPs under evaluation.

The first-order kinematic model of the fixed-wing UAV considered for the analysis is described by the following equations [47]:

$$\begin{aligned} \dot{x}_i &= v_i sin\psi_i, \\ \dot{y}_i &= v_i cos\psi_i, \\ \dot{\psi}_i &= \frac{g \tan\phi_i}{v_i}, \\ \dot{v}_i &= \frac{1}{\alpha_v}\left(v_i^c - v_i\right), \\ \dot{\phi}_i &= \frac{1}{\alpha_\phi}\left(\phi_i^c - \phi_i\right), \end{aligned} \tag{1}$$

where (x_i, y_i), ψ_i, v_i, and ϕ_i are the i-th UAV inertial position, heading angle, speed, and roll angle, respectively; v_i^c and ϕ_i^c are the commanded speed and roll angle, respectively; and α_v and α_ϕ are positive constants.

Additionally, due to the thrust and roll angle limitations of fixed-wing UAVs, the following constraints are imposed on each UAV:

$$\begin{aligned} 0 < v_{min} \leq v_i \leq v_{max}, \\ -\phi_{max} \leq \phi_i \leq \phi_{max}, \\ -\dot{v}_{max} \leq \dot{v}_i \leq \dot{v}_{max}, \\ -\dot{\phi}_{max} \leq \dot{\phi}_i \leq \dot{\phi}_{max}, \end{aligned} \tag{2}$$

where ϕ_{max}, $\dot{v}_{max}$, and $\dot{\phi}_{max} > 0$.

2) MPC-BASED DISTRIBUTED UAV FORMATION CONTROL STRATEGY

The MPC-based controller described in [34] adopts a virtual point tracking approach for UAV formation control. Virtual point tracking uses a virtual moving reference point, O_r, that follows a preloaded reference trajectory during the mission execution. Fig. 2 shows O_r in a typical delta UAV formation. The reference trajectory at time step n is uniquely determined by the position, (x_r, y_r), of the reference point, O_r, and the velocity vector (v_r, ψ_r), where v_r is the reference speed and ψ_r is the reference heading angle. Thus, the SI vector, $\mathbf{x}_n^r$, is defined as:

$$\boldsymbol{x}_n^r = [x_r, y_r, v_r, \psi_r]^T . \tag{3}$$

The UAV that knows the reference trajectory in advance (source/leader UAV in Fig. 2) disseminates $\mathbf{x}_n^r$ by transmitting an SI message at fixed time intervals nt_d, where t_d is the SI dissemination period.

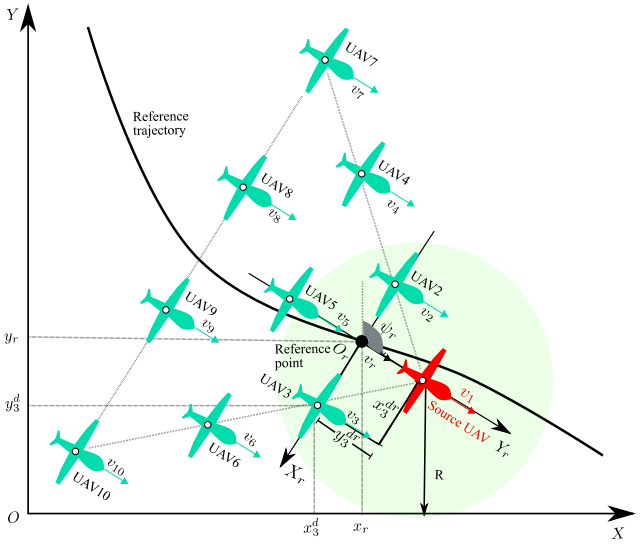

FIGURE 2. Delta UAV formation in the reference point coordinate system $X_rO_rY_r$. R is the radio range of the UAVs transceivers. (x_3^{dr}, y_3^{dr}) is UAV3 desired position referred to the rotated coordinate system $X_rO_rY_r$. (x_3^d, y_3^d) is UAV3 desired position referred to the fixed coordinate system XOY.

Ideally, SI messages must timely reach each UAV in the formation. However, an SI message might require several hops to reach the UAVs that are located farther away from the source (e.g., UAV7 to UAV10 in Fig. 2). In this work, UAVs flying in formation are grouped into M levels according to their longitudinal distances from the source UAV. For example, in Fig. 2, the first level includes the source UAV (UAV1); the second level includes UAV2 and UAV3; the third level consists of UAV4, UAV5, and UAV6; and so on. Note in Fig. 2 that the number of hops required for the SI to reach a particular UAV is directly related to its level group (at least for the transceiver radio range assumed in this figure).

The formation structure in Fig. 2 can be defined in terms of the rotating coordinate system $X_rO_rY_r$ such that in each sampling period the moving reference point is located at O_r. In this coordinate system, each of the UAVs (e.g., the i-th UAV) in the formation must try to maintain the desired reference position (x_i^{dr}, y_i^{dr}) during the mission execution. As the rotated coordinate system $X_rO_rY_r$ changes in each sampling period (i.e., the reference point is moving), it is better to calculate the desired position (x_i^d, y_i^d) of each UAV referred to a fixed XOY coordinate system. Thus, each UAV position (x_i^{dr}, y_i^{dr}) in the $X_rO_rY_r$ coordinate system is transformed to

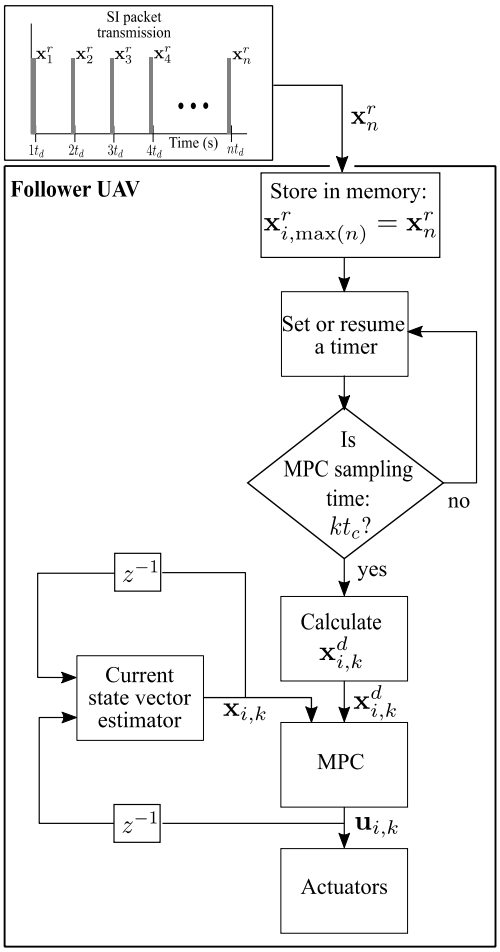

FIGURE 3. Formation control scheme of each follower UAV.

the (x_i^d, y_i^d) position in the fixed XOY system by using:

$$\begin{bmatrix} x_i^d \\ y_i^d \end{bmatrix} = \begin{bmatrix} x_r \\ y_r \end{bmatrix} + \begin{bmatrix} cos\psi_r & sin\psi_r \\ -sin\psi_r & cos\psi_r \end{bmatrix} \begin{bmatrix} x_i^{dr} \\ y_i^{dr} \end{bmatrix}, \tag{4}$$

where (x_r, y_r) and ψ_r (defined as positive clockwise) are given referred to the XOY system.

The MPC control law requires that each follower UAV has a formation control scheme, such as the one depicted in Fig. 3. In this scheme, the i-th follower UAV that receives a message containing the SI vector, $\mathbf{x}_n^r$, stores the reference position, (x_r, y_r); reference speed, v_r; and reference heading angle, ψ_r, in an $\mathbf{x}_{i,\max(n)}^r$ vector. Thus, $\mathbf{x}_{i,\max(n)}^r$ contains the latest SI vector that is received. Then, after setting a timer to wait for the next MPC controller sampling period, kt_c, the i-th UAV calculates a desired state vector $\mathbf{x}_{i,k}^d = \left[x_{i,k}^d, y_{i,k}^d, v_{r,k}, \psi_{r,k}\right]^T$ by substituting the content of $\mathbf{x}_{i,\max(n)}^r$ in (4) to obtain $(x_{i,k}^d, y_{i,k}^d)$. Then, $\mathbf{x}_{i,k}^d$ is fed to the MPC block together with the estimated current state vector, $\mathbf{x}_{i,k} = \left[x_{i,k}, y_{i,k}, v_{i,k}, \psi_{i,k}\right]^T$. This vector contains the estimated current position, $(x_{i,k}, y_{i,k})$; speed, $v_{i,k}$; and heading angle, $\psi_{i,k}$ of the i-th UAV. For every MPC controller sampling period, kt_c, the MPC provides an actuator control vector, $\mathbf{u}_{i,k} = \left[v_{i,k}^c, \phi_{i,k}^c\right]^T$, which is obtained by minimizing a cost function over a discrete time period Nt_c, where N is called the predictive horizon. The cost function includes $\mathbf{x}_{i,k}^d$ and $\mathbf{x}_{i,k}$, along with predicted state and control vectors, $\mathbf{x}_{i,k+s+1|k}$ and $\mathbf{u}_{i,k+s|k}$, covering the predictive horizon (i.e., $s = 0, 1, 2, \ldots, N$), which are calculated locally as part of the optimization process. Once $\mathbf{u}_{i,k}$ has been obtained, it is fed to the UAV actuators with the aim of maintaining the formation (i.e., $\mathbf{u}_{i,k}$ is sent to the UAV actuators which convert the speed, v_i^c, and roll angle, ϕ_i^c, commands into mechanical motion). Note that the SI dissemination period, t_d, is not restricted to be equal to the MPC controller sampling period, t_c; thus, it is possible to disseminate SI more frequently. It is important to mention that, different from [34], no obstacle or inter-UAV collision avoidance was included in the evaluation framework implementation. This was done to focus the analysis on studying UAV formation deviations that are caused by the network performance of different MBPs while disseminating SI. For the sake of brevity, the reader is referred to [34] for more details about the MPC strategy used in the evaluation framework.

It is important to timely receive SI messages for the proper operation of the distributed control strategy. To explain this, consider that $t_d = t_c$. Under this assumption, if the SI vector corresponding to sampling time k, $\mathbf{x}_k^r$, is not received by the i-th UAV (e.g., the SI packet was lost) or if it is received after kt_c (e.g., the SI packet arrival was delayed), then will have to be calculated using the current value of $\mathbf{x}_{i,\max(n)}^r$, where $\max(n) < k$. Note that $\max(n)$ is the discrete-time index of the latest SI vector that is successfully received (not necessarily $\max(n) = k - 1$). Therefore, depending on the trajectory followed, a UAV can experience slight deviations from its intended flight path that are caused by packet delays and losses. Furthermore, if the deviations are large enough, the UAV could get out of radio coverage and get completely lost. Thus, it is important to analyze the suitability of different MBPs to disseminate the SI within a FANET and the effects that common ad-hoc networking impairments (e.g., packet loss and delay) might have on losing UAV formation. The next subsection provides a brief introduction to the different MBP strategies evaluated in this work.

B. MULTI-HOP BROADCAST PROTOCOLS (MBPs)

Often, it has been assumed that the SI for distributed UAV formation control can be disseminated by employing multi-hop communications. An MBP operates at the network layer, and its primary goal is to timely deliver information from a source node (e.g., leader UAV) to all nodes or a subgroup of nodes that are located in a zone of relevance. However, when using MBPs, the SI dissemination process will experience packet losses, variable delays, and other factors inherent to FANETs. Thus, a drop in the MBP network performance might negatively impact the effectiveness of the distributed UAV formation control strategy in maintaining the formation. In this sense, an MBP is commonly evaluated by considering

its average network efficiency in terms of the overhead, delay, and packet delivery ratio. However, in order to assess its suitability for SI message dissemination, the MBP performance should be weighed according to its impact on the controller effectiveness at maintaining the flight formation during a mission execution.

A straightforward way to address SI dissemination in FANETs would be to implement a Simple Flooding dissemination mechanism. In this mechanism, each node that receives a message for the first time retransmits it with no further restrictions. Note that Simple Flooding is inefficient in terms of network performance. In ad-hoc networks with high node density, using Simple Flooding results in over-occupancy of the radio channel resources, higher communication overhead, increased contention and packet collisions, which is referred to as the broadcast storm problem (BSP) [36].

There are different proposals in the literature focused on developing more efficient MBPs than Simple Flooding for multi-hop ad hoc networks, such as MANETs [41] and VANETs [35], [37]. In this sense, FANETs can be considered to be a subgroup of VANETs, which are a subgroup of MANETs. Thus, it is natural to use MBPs that were previously developed for MANETs and VANETs to address multi-hop broadcast dissemination within FANETs. However, it is necessary to study if the network performance offered by different MBP strategies enables the distributed UAV formation controller to maintain flight formation during a mission execution. To this end, representative protocols of different approaches used in multi-hop broadcasting for MANETs and VANETs were selected and implemented in the evaluation framework that is proposed in this work. Specifically, Simple Flooding [35], Distance-Based [35], [36], Probability-Based [37], and Counter-Based [36] MBPs were chosen to evaluate their suitability for SI dissemination. The dissemination strategies used by these protocols to address the packet dissemination task are presented in the next subsection.

1) MBPs DESCRIPTION

MBPs use different parameters to select a subset of relay nodes instead of flooding the messages through all intermediate nodes. Regardless of the specific parameters used to make the relay decision, MBPs have the generic architecture shown in Fig. 4. The SI broadcasted by the leader is handed to the MBP at delivery point 1 (DP1) in Fig. 4. The protocol makes the relay/drop decision according to the dissemination strategy used. MBPs share similar problems related to the physical (PHY) and multiple access control (MAC) layers. However, there are some issues that have specific dissemination strategies tailored to address them. To better explain these issues, the dissemination strategies used by the MBPs that are evaluated in this work are discussed next.

The Simple Flooding protocol [35] implements a procedure where each node will instantly rebroadcast a message after receiving it for the first time. If duplicated messages are received, they will not be rebroadcasted.

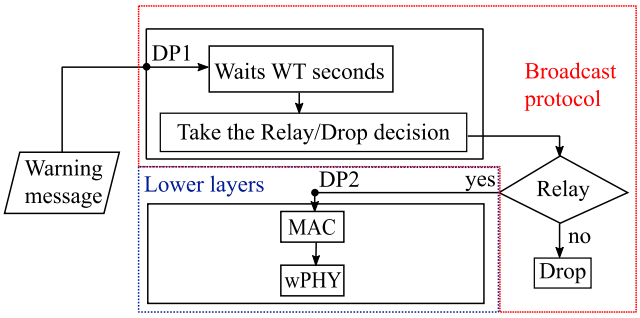

FIGURE 4. MBP generic architecture.

The Distance-Based MBP introduced in [36] (hereafter referred to DTh-Distance-Based protocol) aims to maximize the additional coverage that each potential relay node provides. To achieve this, when a node j receives a particular broadcast message for the first time, it estimates the relative distance, d_{ij}, between the node sending the message and itself. Afterwards, node j compares d_{ij} to a predefined distance threshold, D. If $d_{ij} < D$, the transmission is canceled; otherwise, the node j waits for a random waiting time, RT, before attempting to rebroadcast the message. If during the waiting period, RT, node j receives a duplicated broadcast message, it estimates the relative distance, $\hat{d}_{ij}$, between the node that transmitted the duplicated message and itself. Then, if $\hat{d}_{ij} < d_{ij}$, node j updates $d_{ij} = \hat{d}_{ij}$; otherwise, the value of d_{ij} is kept. If $d_{ij} < D$ the transmission is canceled; otherwise, RT is resumed. If another duplicated message is received before RT expires, the procedure described before must be repeated. If the waiting time expires and the current $d_{ij} > D$, node j rebroadcasts the message. All duplicated messages that are received after RT expires are discarded.

In the Distance-Based MBP introduced in [35] (hereafter referred as a WT-Distance-Based protocol), a node j that receives a message for the first time listens for duplicate messages during a waiting period, WT. If during this period a duplicate message is received by node j, the message is discarded, and node j does not rebroadcast the information. If WT expires and no duplicate is received, the message is rebroadcasted by node j. The waiting time, WT, is calculated by using:

$$WT = -\frac{MaxWT}{R} d_{ij} + MaxWT, \tag{5}$$

where d_{ij} is the relative distance between the sender node (e.g., node i) and node j, $MaxWT$ is the maximum waiting time, and R is the radio range of the transceivers. Therefore, the node that is farther away from the sender will have the shortest WT and hence the higher priority to rebroadcast the message.

The Probabilistic-Based protocol introduced in [37] assigns a higher relaying probability to nodes that are located farther away from the current sender. To do this, when a node

j receives a particular broadcast message for the first time, it estimates (e.g., based on RSSI measurements or GPS coordinates) the relative distance, d_{ij}, between the node sending the message and itself. Then, a forwarding probability, p_{ij}, is calculated as follows:

$$p_{ij} = \frac{d_{ij}}{R}, \tag{6}$$

where R is the transceiver radio range. Before node j attempts to rebroadcast the message, it listens for duplicate broadcasts during the waiting time, WT. If during WT node j receives a duplicate broadcast, it estimates its relative distance, $\hat{d}_{ij}$, from the node that sent the duplicate. Then, a probability, $\hat{p}_{ij}$, is calculated by substituting $\hat{d}_{ij}$ in (6). If $\hat{p}_{ij} < p_{ij}$, then node j updates its forwarding probability to $p_{ij} = \hat{p}_{ij}$; otherwise, the current value of p_{ij} is kept. Once WT expires, node j can rebroadcast the message with a probability of p_{ij}. If the message is not rebroadcasted, then the message is buffered by an additional period, δ. If a rebroadcast from the message is received before δ expires, the message is discarded from the buffer and node j does not perform a rebroadcast. Otherwise, node j rebroadcasts the packet with $p_{ij} = 1$. The additional waiting time δ (which is typically less than WT) accounts for one-hop transmissions and propagation delays.

The Counter-Based protocol introduced in [36] (hereafter referred to as the C-Counter-Based protocol) prevents a node from rebroadcasting after receiving the same message C times. To achieve this, when a node j receives a particular broadcast message for the first time, a counter, c, is initialized. Afterward, node j waits a random waiting time, RT, before attempting to rebroadcast the message. If during RT node j receives a duplicate message, c is increased by one. If $c < C$, where C is a counter threshold, the waiting is resumed. Otherwise, the rebroadcast of the message is canceled. If $c < C$ after WT expires, the message is rebroadcasted by node j.

IV. PROBLEM STATEMENT

As mentioned before, when designing distributed UAV formation control strategies, it is commonly assumed that the SI dissemination problem is somehow solved. That is, from the controller perspective, MBPs can be seen as a black box that causes random packet losses and delays for the disseminated SI message. However, different MBPs use different strategies to address the SI dissemination task. Thus, the network performance that is provided by different MBPs may differently affect the ability of the control strategy to maintain the UAV formation.

When an MBP is used for SI dissemination, packet loss and packet delivery delay variability will likely be present during the dissemination process since both are inherently present in ad-hoc networks and hence in FANETs [22]. These factors could affect the controller ability to maintain the UAV formation in different ways. Furthermore, it can be inferred that if both, the packet loss and packet delivery delay variability, are large enough, a UAV might deviate from its expected course and even break away from the formation. Nevertheless, it is not clear beforehand how the network performance offered by a particular MBP will affect the controller ability to maintain the formation. Evaluating this is not a trivial task since a packet can experience delays that are caused by issues such as the number of hops, MAC contention, and retransmissions. Similarly, a packet can get lost because of PHY impairments, MAC drops, inhibited retransmissions by the MBP, etc. Hence, it is necessary to analyze this problem that, to the best of our knowledge, has not been addressed before.

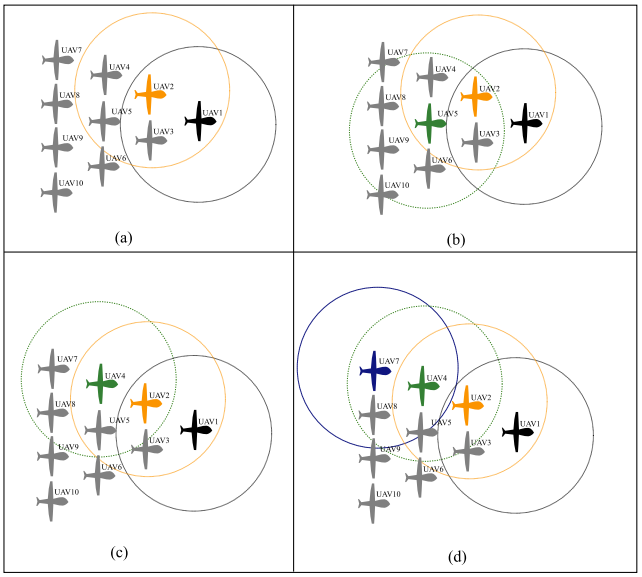

FIGURE 5. Multihop SI message dissemination with an arbitrary MBP.

For example, consider the scenario shown in Fig. 5 where the leader UAV (UAV1) broadcasts an SI message. The UAVs in the second level (UAV2 and UAV3) receive the message, and using the MBP, they decide that UAV2 will rebroadcast the SI packet (Fig. 5(a)). The rebroadcasted SI message is overheard by UAV1 and the other node in the same level (UAV3); thus, the MBP hinders the retransmission from UAV1 or the rebroadcast from UAV3. In the next step, note that if UAV5 rebroadcasts the SI packet (Fig. 5(b)), all the UAVs in the third and fourth levels should be able to receive it. Contrastingly, if UAV4 rebroadcasts the SI packet (Fig. 5(c)), then UAV10 will not receive the SI message. Furthermore, if UAV7 rebroadcasts the SI packet, UAV10 will not receive the SI message in the current sampling period (Fig. 5(d)). This example helps to highlight one of the issues that may arise while disseminating SI messages through a FANET by means of an MBP. Since a particular MBP could provide low SI dissemination delays while another MBP may offer a better packet delivery ratio or less overhead, it is necessary to provide a common evaluation framework to assess the suitability of different MBPs for SI dissemination in distributed UAV formation control applications.

Now, assume that the SI dissemination period, t_d, and the MPC controller sampling period, t_c, are equal. Under an ideal SI dissemination assumption, all SI messages, $\mathbf{x}_n^r$, that

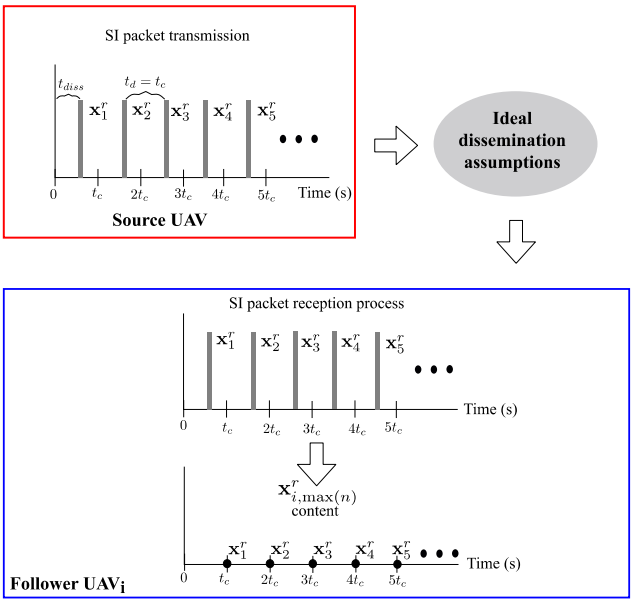

FIGURE 6. Reception of SI messages under an ideal SI dissemination assumption. $\mathbf{t_d}$ is the dissemination period and $\mathbf{t_c}$ is the MPC controller sampling period. $\mathbf{x_n^r}$ is the SI vector that receives the i-th follower UAV. $\mathbf{x_{i,max(n)}^r}$ is the latest $\mathbf{x_n^r}$ vector stored. Note in this figure that $\mathbf{t_d = t_c}$ with $\mathbf{n = k}$.

originated from the source UAV will timely arrive at the i-th follower UAV without packet losses, as shown in Fig. 6. From Section III-A, recall that the variable $\mathbf{x}^r_{i,\max(n)}$ contains the latest SI vector that is successfully received by the i-th UAV. Now let $\mathbf{x}^r_{i,\max}(t)$ represent the content of vector $\mathbf{x}^r_{i,\max(n)}$ in continuous time. Note that, for $t > mt_c$, $\mathbf{x}^r_{i,\max}(t) = \mathbf{x}^r_m$ if $\mathbf{x}^r_m$ was successfully received and no SI packet is received in the time interval $(mt_c, t]$. Now assume that the leader UAV disseminates the k-th SI packet, $\mathbf{x}^r_k$, at time

$$(k-1)\,t_c + t_{diss} \tag{7}$$

where t_{diss} is a fixed period such that $0 < t_{diss} < t_c$. Under ideal dissemination conditions, we have:

$$\boldsymbol{x}^r_{i,max}\left((k-1)\,t_c + t_{diss}\right) = \boldsymbol{x}^r_k \tag{8}$$

where $(k-1)\,t_c + t_{diss} < kt_c$. Since no additional SI packet is generated by the leader in the time interval $((k-1)\,t_c + t_{diss}, kt_c + t_{diss})$, at sampling time kt_c, we have:

$$\boldsymbol{x}^r_{i,max}(kt_c) = \boldsymbol{x}^r_k = \mathbf{x}^r_{i,max(n)}. \tag{9}$$

This implies that, under the ideal dissemination assumption, the k-th SI message, $\mathbf{x}^r_k$, will be used by the controller at sampling time kt_c to calculate the desired state vector, $\mathbf{x}^d_{i,k}$, and the actuator control vector, $\mathbf{u}_{i,k}$.

When an actual MBP is used for SI dissemination, the i-th UAV will receive the k-th SI packet after experiencing some random delay, $t^{delay}_{i,k}$. Thus, if the k-th SI packet is delayed by $t^{delay}_{i,k}$ and no SI message newer than $\mathbf{x}^r_k$ is received within time interval $\left((k-1)t_c + t_{diss}, (k-1)t_c + t_{diss} + t^{delay}_{i,k}\right)$, we have:

$$\boldsymbol{x}^r_{i,max}\left((k-1)t_c + t_{diss} + t^{delay}_{i,k}\right) = \boldsymbol{x}^r_k \tag{10}$$

where $0 < t^{delay}_{i,k} < \infty$ is a random variable. Thus, at the k-th controller sampling time, we have:

$$\boldsymbol{x}^r_{i,max}(kt_c) = \begin{cases} \boldsymbol{x}^r_k, & t^{delay}_{i,k} < t_c - t_{diss} \\ \boldsymbol{x}^r_{i,max}\left((kt_c)^-\right), & t^{delay}_{i,k} > t_c - t_{diss} \end{cases} \tag{11}$$

where $\boldsymbol{x}^r_{i,max}\left((kt_c)^-\right)$ is the latest SI packet stored in $\mathbf{x}^r_{i,\max(n)}$ prior to $t = kt_c$. Note that if $t^{delay}_{i,k} > t_c - t_{diss}$, then $\max(n) < k$ at time $t = kt_c$, but this does not imply that $\mathbf{x}^r_{i,\max(n)} = \mathbf{x}^r_{k-1}$ since the latest SI vector that is successfully received by the i-th UAV is not necessarily $\mathbf{x}^r_{k-1}$.

In addition to delays, an SI packet can experience packet drops, MAC collisions or reception errors caused by impairments at the PHY layer. For notational convenience, let us define:

$$t^{Rx}_{i,k} = (k-1)\,t_c + t_{diss} + t^{delay}_{i,k}. \tag{12}$$

Then, if $\alpha_{i,k}$ is an indicator random variable accounting for the proper reception of $\mathbf{x}^r_k$ by the i-th UAV and no SI message newer than $\mathbf{x}^r_k$ is received within the time interval $\left((k-1)t_c + t_{diss}, t^{Rx}_{i,k}\right)$, we have:

$$\boldsymbol{x}^r_{i,max}\left(t^{Rx}_{i,k}\right) = \alpha_{i,k}\boldsymbol{x}^r_k + \left(1-\alpha_{i,k}\right)\boldsymbol{x}^r_{i,max}\left(\left(t^{Rx}_{i,k}\right)^-\right)\ldots \tag{13}$$

where $\alpha_{i,k} = \{0, 1\}$, and $\mathbf{x}^r_{i,max}\left(\left(t^{Rx}_{i,k}\right)^-\right)$ is the latest SI packet stored in $\mathbf{x}^r_{i,\max(n)}$ prior to $t = t^{Rx}_{i,k}$. Therefore, at sampling time kt_c, we have:

$$\boldsymbol{x}^r_{i,max}(kt_c) = \begin{cases} \alpha_{i,k}\boldsymbol{x}^r_k + \left(1-\alpha_{i,k}\right)\boldsymbol{x}^r_{i,max}\left((kt_c)^-\right), & t^{Rx}_{i,k} < kt_c \\ \boldsymbol{x}^r_{i,max}\left((kt_c)^-\right), & t^{Rx}_{i,k} > kt_c \end{cases} \tag{14}$$

Hence, the controller will use $\mathbf{x}^r_k$ at sampling time kt_c to calculate $\mathbf{x}^d_{i,k}$ and $\mathbf{u}_{i,k}$ if the MBP and packet transmission impairments (at the PHY and MAC layers) enable:

$$t^{delay}_{i,k} < t_c - t_{diss} \quad \text{and } \alpha_{i,k} = 1. \tag{15}$$

The statistics of both $t^{delay}_{i,k}$ and $\alpha_{i,k}$ depend on the particularities of the dissemination strategy used by the MBP, the position of the i-th UAV within the formation, the MAC used by the transceivers, the number of hops needed by the SI packet to reach the i-th UAV, and the wireless channel impairments, which may be different for each hop. Closed expressions for both random variables are extremely hard to find since they capture all possible impairments that are experienced by an SI packet while wirelessly hopping from the leader UAV to the i-th UAV. For this reason, the evaluation of MBPs usually relies on simulations to calculate network metrics such as the packet delivery ratio and packet delay.

When comparing the performance of different MBPs, these metrics are commonly calculated by averaging over all the nodes forming an ad-hoc network. Nevertheless, as explained in the next sections, for the analysis presented in this paper, it is relevant to obtain these metrics for a single UAV, especially those that are located further away from the leader UAV.

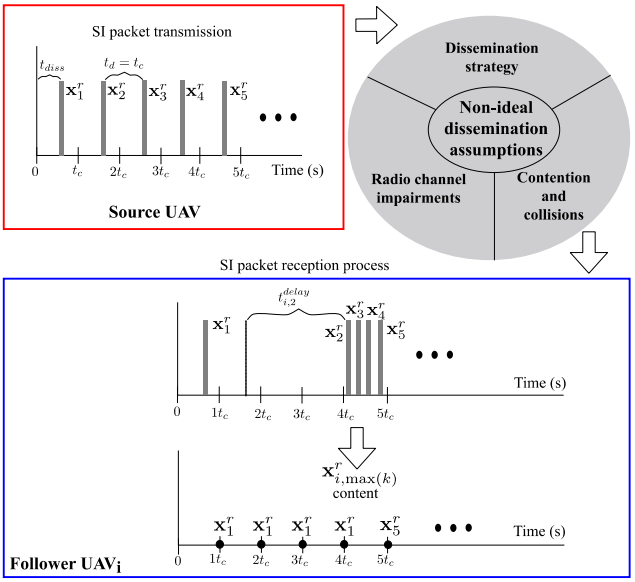

(a)

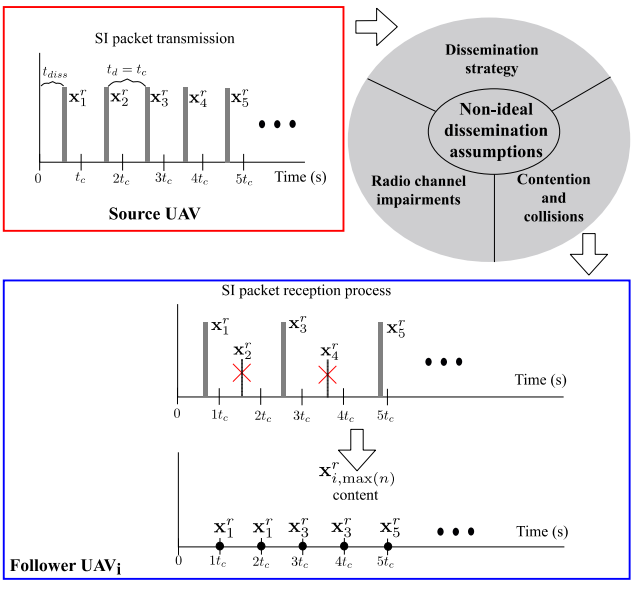

(b)

FIGURE 7. Representation of the SI packet losses and delays that can occur when using an MBP for SI dissemination. t_d is the dissemination period and t_c is the MPC controller sampling period. $\mathbf{x}_n^r$ is the SI vector that receives the i-th follower UAV. $\mathbf{x}_{i,\max(n)}^r$ is the latest $\mathbf{x}_n^r$ vector stored. Note in this figure that $t_d = t_c$ with $n = k$.

Fig. 7 shows two examples of the reception of SI messages in the i-th UAV when packet loss and delays are present in the dissemination process. Note in this figure the critical role that MBPs can play when used for SI dissemination in distributed UAV formation control applications. For example, in Fig. 7(a), $\mathbf{x}_2^r$, $\mathbf{x}_3^r$, and $\mathbf{x}_4^r$ SI packets are received slightly after $4t_c$, i.e., $4t_c < t_{i,2}^{Rx}, t_{i,3}^{Rx}, t_{i,4}^{Rx} < 5t_c$. Thus, the controller has to use $\mathbf{x}_{i,\max(n)}^r = \mathbf{x}_1^r$ to calculate $(\mathbf{x}_{i,2}^d, \mathbf{u}_{i,2})$, $\left(\mathbf{x}_{i,3}^d, \mathbf{u}_{i,3}\right)$, and $(\mathbf{x}_{i,4}^d, \mathbf{u}_{i,4})$. This is equivalent to losing $\mathbf{x}_2^r$, $\mathbf{x}_3^r$ and $\mathbf{x}_4^r$ since $\mathbf{x}_5^r$ was received timely, i.e., $t_{i,5}^{Rx} < 5t_c$, and is used to calculate $(\mathbf{x}_{i,5}^d, \mathbf{u}_{i,5})$. In contrast, in Fig. 7(b), $\mathbf{x}_2^r$ and $\mathbf{x}_4^r$ are lost (i.e., $\alpha_{i,2} = 0$ and $\alpha_{i,4} = 0$) but $\mathbf{x}_1^r$, $\mathbf{x}_3^r$, and $\mathbf{x}_5^r$ are timely received (i.e., $t_{i,1}^{Rx} < t_c$, $t_{i,3}^{Rx} < 3t_c$, and $t_{i,5}^{Rx} < 5t_c$). Then, compared to Fig. 7(a), in Fig. 7(b), the controller calculates $\left(\mathbf{x}_{i,2}^d, \mathbf{u}_{i,2}\right)$ using $\mathbf{x}_1^r$, $\left(\mathbf{x}_{i,3}^d, \mathbf{u}_{i,3}\right)$ using $\mathbf{x}_3^r$, and $(\mathbf{x}_{i,4}^d, \mathbf{u}_{i,4})$ using $\mathbf{x}_3^r$. Therefore, an MBP offering high packet delivery ratio but large delays (i.e., the SI is not timely disseminated) might provide a performance similar to that obtained with an MBP offering an inferior packet delivery ratio but lower delays.

From the previous discussion, it can be asserted that choosing or designing a particular MBP aimed at disseminating SI for distributed UAV formation control is not a trivial task. Thus, an evaluation methodology to assess the suitability of the MBPs for SI dissemination in FANETs is proposed in the following section. Then, the proposed methodology is used to evaluate the performance of the representative MBPs that were introduced in the previous section.

V. EVALUATION METHODOLOGY

This section introduces the evaluation methodology developed to study the effects of the SI dissemination process in the multi-UAV formation control strategy. Traditionally, metrics such as the packet delivery ratio (PDR) and dissemination delay are used to evaluate and compare the performance of multi-hop broadcast protocols. However, metrics aimed at measuring the impact of the MBP on the flight formation have to also be considered. For this purpose, in addition to network metrics, the use of trajectory metrics is proposed in this paper. Specifically, this work considers the root mean square (RMS) error between the ideal and actual trajectories of each UAV and the number of lost UAVs. Thus, the proposed methodology allows to compare the performance of different dissemination strategies in terms of: a) trajectory metrics such as the RMS error and the number of lost UAVs; and b) network metrics such as the PDR.

To implement the evaluation methodology, an evaluation framework based on the well-known OMNeT++ network modeler [48], MATLAB®, and the ACADO toolkit [49] was developed. The software that was developed for the framework includes C++ scripts and MATLAB® code, which can be provided to the interested reader upon request.

The following subsections elaborate on the evaluation scenario, the performance metrics used, and the design and implementation details of the evaluation framework.

A. EVALUATION SCENARIO

Within the evaluation scenario, it is necessary to first define the U2U link and flight parameters that are used in each trial.

Another variable to consider is the reference trajectory of the multi-UAV mission. In particular, it is important to define a trajectory (within the kinematic capabilities of the UAV) that enables differentiating the performance provided by the MBPs under evaluation, which is done in order to obtain relevant conclusions regarding the suitability of the MBPs for SI dissemination.

1) U2U LINK PARAMETERS

One of the most relevant considerations when evaluating communication protocols is to define the wireless propagation conditions. Thus, the radio channel propagation model introduced in [50], that was designed for U2U radio links, was implemented within the evaluation framework.

Another parameter to consider is the wireless technology used by the transceiver. Different technologies have been proposed to enable U2U communications such as IEEE 802.11a/b/g/n, IEEE 802.15.4, 3G/LTE, and infrared [8]. However, several FANET proposals rely on the IEEE 802.11p standard [51], which is the most prominent option for VANETs. The IEEE 802.11p standard was specifically designed for VANET deployments where the nodes have high mobility, speed, and acceleration. Since these characteristics are also observed in FANET deployments, the evaluation scenario considers the use of IEEE 802.11p transceivers to enable U2U communications. Table 1 summarizes the values of each variable used by the 802.11p transceivers considered within the evaluation framework.

TABLE 1. Parameters of the U2U 802.11p transceivers considered in the evaluation scenario.

General parameters	
Wireless technology	IEEE 802.11p
Base frequency	5.880 GHz
Data rate[1]	3 Mbps
Nominal radio range R	200 m
Reachable radio[2] RR	300 m

2) FLIGHT PARAMETERS

The UAVs mobility is ruled by three main factors within the evaluation scenario: 1) the kinematic model defined in subsection III-A-1; 2) the distributed formation control strategy discussed in subsection III-A-2; and 3) the control constraints that are defined considering the typical specifications found in commercial UAVs. Table 2 provides the values that are used by the kinematic model and the MPC controller in the evaluation scenario. These values were chosen such that realistic fixed-wing UAV movements are generated within the simulation testbed (e.g., smooth turns and speed changes).

[1]The data rate is chosen to be the lowest supported by this standard, i.e., 3 Mbps. This is because the modulation used for this data rate fulfills the data rate requirements and offers better power efficiency.

TABLE 2. Values used in the kinematic model for the fixed-wing UAV and the MPC controller.

Symbol	Kinematic model parameters	
v_r	Reference speed	{15, 17.5, 20, 22.5, 25, 27.5} m/s
l_d	Lateral distance	100 m
L_d	Longitudinal distance	100 m
v_{min}	Minimum velocity	2 m/s
v_{max}	Maximum velocity	40 m/s
$\dot{v}_{max}$	Maximum acceleration	2 m/s^2
ϕ_{max}	Maximum roll angle	40 deg
$\dot{\phi}_{max}$	Maximum roll angle speed	40 deg/s
	MPC parameters [34]	
t_N	Prediction horizon time	2.5 s
t_c	Sampling period	0.5 s

3) FLIGHT TRAJECTORIES

When performing a multi-UAV mission, a distributed UAV flight formation controller aims to keep all UAVs within the formation. Thus, the trajectory that is followed during the mission is of particular relevance to evaluate the control strategy effectiveness. Note, a sinuous trajectory will be a harder challenge for the controller than a simple straight line. Thus, to adequately measure the effectiveness of the SI dissemination process in the formation controller performance, special attention should be paid to the UAV's trajectory selection.

One of the most relevant applications of multi-UAV systems is in missions involving sweeping large geographic areas at once for data-gathering, e.g., multispectral and visual data. Commonly, for this kind of task, the area to be covered by the UAVs is divided into several straight paths or rows [52], [53], which is known as a sweep trajectory [54]. In this trajectory, at the end of each row, the UAVs make a U-turn outside the area of interest to follow the next row, as shown in Fig. 8. This sweep trajectory was considered as the reference trajectory within the evaluation scenario. Thus, since the MPC controller implemented in this work uses virtual point tracking (see subsection III-A-2), during each trial, the UAVs will try to keep their relative distance from the virtual point while they follow the sweep trajectory (Fig. 8) at a fixed speed.

B. PERFORMANCE METRICS

To assess the suitability of a particular MBP for SI dissemination in UAV formation control scenarios, two kinds of metrics are considered:

1) Metrics that measure the deviation between the ideal and actual trajectories that are followed by each UAV when using a particular MBP.
2) Metrics related to the performance of each MBP from a networking point of view.

These metrics are explained next.

[2]Beyond the reachable radio, RR, it is assumed that none of the UAVs can sense and receive packets since there is high communication degradation.

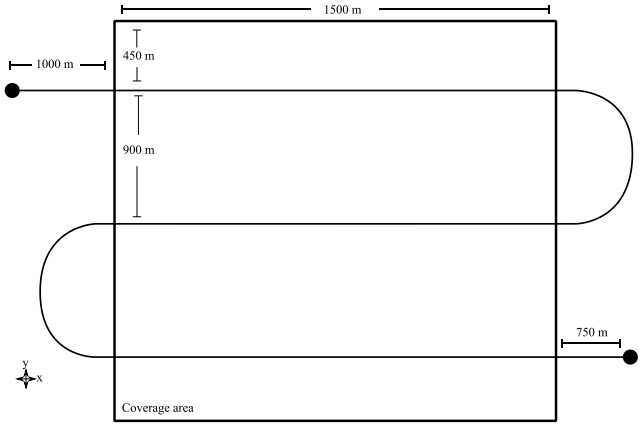

FIGURE 8. Sweep trajectory considered in the evaluation scenario. It is assumed that the trajectory starting point is coordinate $(\mathbf{x_{r0}}, \mathbf{y_{r0}}) = [750, 2000]$ m with a heading angle of $\psi_{\mathbf{r0}} = 90$ deg. At the beginning of each trial, the UAV formation follows a straight line measuring 2500 m. A simulation warm-up period is considered where no metrics are collected for the first 1000 m of this straight line. The trajectory includes U-turns following a semicircle with a diameter equal to 900 m.

1) TRAJECTORY METRICS

The trajectory metrics provide information regarding how close each UAV follows its ideal path during a mission execution. It is important to highlight that, depending on its objective, significant deviations from the ideal paths could compromise a multi-UAV mission. Furthermore, a particular UAV could get lost if the deviation from its ideal path is large enough at certain points in the trajectory. Thus, within the evaluation framework, the actual path that is followed by each UAV in each trial is recorded in order to obtain the following metrics:

1) *Path Root Mean Square Error (P-RMSE).* The P-RMSE measures the root mean square error between the ideal and actual trajectories of each UAV. Thus, the P-RMSE helps to quantify the performance of the SI dissemination strategy in terms of the trajectory errors that should be addressed by the controller. Specifically, in each trial, the P-RMSE$_i$ of the i-th UAV is calculated as:

$$P\text{-}RMSE_i = \sqrt{\frac{\sum_{k=1}^{S}[(x_i^{ac}[k]-x_i^{de}[k])^2+(y_i^{ac}[k]-y_i^{de}[k])^2]}{S}}, \tag{16}$$

where $\left(x_i^{ac}[k], y_i^{ac}[k]\right)$ is the i-th UAV actual position at sample time k, $\left(x_i^{de}[k], y_i^{de}[k]\right)$ is the i-th UAV desired (ideal) position at sample time k, and S is the total number of samples considered in the simulation. The average P-RMSE is then defined as:

$$P\text{-}RMSE = \frac{1}{\lambda_3}\sum_{i\in S_{\lambda_3}} P\text{-}RMSE_i, \tag{17}$$

where S_{λ_3} is the subset of UAVs that are located in level three and above in the formation, and λ_3 is the total number of UAVs belonging to S_{λ_3}. Note that the P-RMSE does not consider the error generated once a particular UAV is considered definitively lost.

2) *Lost UAVs (LU).* This measures the number of UAVs whose deviation from the ideal path leaves them definitely outside the wireless range of any other UAV that is still within the formation. Thus, the LU metric is used to weigh the trajectory errors measured by the P-RMSE. The LU metric is calculated by counting the number of UAVs that, at some point during the simulation, are outside a reachable ratio, RR, which is defined as:

$$RR = d_{max} + 1.5R, \tag{18}$$

where R is the nominal radio range, and d_{max} is the distance between the source UAV and the follower UAVs that are located farther away but are still within the formation. It is important to mention that once a particular UAV is outside the *RR*, it is considered definitively lost, even though it might rejoin the formation by chance (e.g., the flight path followed by a UAV that is lost in the first curve eventually leads it to encounter the UAV formation after the second U-turn).

2) NETWORK METRICS

Network metrics are used to assess the performance of the SI dissemination process when using a particular MBP. Traditionally, when evaluating the performance of MBPs in ad-hoc networks, it is assumed that the network topology changes over time as nodes move and its one-hop neighborhood changes. Thus, the number of hops that a message needs to perform to reach a particular node varies over time. Note that for the problem under study in this work this is not necessarily the case, especially if the distributed UAV formation control strategy is working properly. This is particularly true for the nodes that are located in the second level of the formation (see Subsection III-A-2) since the SI will reach all nodes in this level with a single hop from the source UAV. This means that the SI will reach these nodes on-time with a high probability. Thus, if metrics such as the packet delivery ratio are calculated considering these nodes, the results may become biased, thus making it challenging to assess the network performance that is experienced by nodes that are located farther away from the source. Therefore, in this work, the network metrics are calculated by considering the nodes needing two hops or more to receive the SI from the source (i.e., level two and higher in the formation). Under this consideration, the network metrics considered in the analysis performed in this paper are introduced next.

a) *Packet Delivery Ratio (PDR).* The PDR is the average number of SI packets (not counting duplicated packets) that are successfully received within the UAV formation. Thus, the PDR measures the overall efficiency of the SI dissemination strategy. For each trial, define $N^i_{SI_{rx}}$ as the number of SI packets that are successfully received by the i-th UAV. Then, the packet delivery

ratio for the i-th UAV, PDR_i, is calculated as:

$$PDR_i = \frac{N^i_{SI_{rx}}}{N_{SI_{tx}}} \tag{19}$$

where $N_{SI_{tx}}$ is the total number of SI messages that are transmitted by the source UAV during a simulation trial. The average PDR is then defined as:

$$PDR = \frac{1}{\lambda_3} \sum\nolimits_{i \in S_{\lambda_3}} PDR_i, \tag{20}$$

where S_{λ_3} is the subset of UAVs that are located in level three and above in the formation, and λ_3 is the total number of UAVs belonging to S_{λ_3}. Note that for the analysis performed in this paper, the UAVs that are located in level 2 are not included in the calculation of the metrics since they are located a single hop from the leader UAV (SI source – level 1).

b) *Average SI age (AvgSIage).* The average SI age (AvgSIage) provides a measure about how ''old'' the SI, $\mathbf{x}^r_{i,\max(n)}$, used by the controller in each controller sampling time, kt_c, is. Thus, the AvgSIage metric measures the quality or ''freshness'' of the SI used by the controller in each sampling period. That is, if

$$\boldsymbol{x}^r_{i,max}\,(kt_c) = \boldsymbol{x}^{\mathbf{r}}_{i,max(n)} \tag{21}$$

then the SI age, $SIage_i\,(\mathrm{k})$, for the i-th UAV at sampling time kt_c is defined as:

$$SIage_i\,(k) = k - max\,(n)_i \tag{22}$$

where $\max\,(n)_{\mathrm{i}}$ is the discrete time index of the latest SI packet that is successfully received by the i-th UAV. Then, the average SI age (AvgSIage) metric for the i-th UAV is defined as:

$$AvgSIage_i = \frac{1}{N_{cst}} \sum\nolimits_{k=1}^{N_{cst}} SIage_i\,(k), \tag{23}$$

where N_{cst} is the number of controller sampling times during a simulation run. For the analysis, it is convenient to define:

$$AvgSIage_{L_m} = \frac{1}{N_{L_m}} \sum\nolimits_{i \in S_{L_m}} AvgSIage_i \tag{24}$$

where S_{L_m} is is the subset of UAVs that are located in level m in the formation, and $\mathrm{J}_{\mathrm{L_j}}$ is the total number of UAVs belonging to S_{L_m}.

c) *Burst average length (BAL).* The BAL metric measures how many consecutive packets (i.e., length) are lost on average. In wireless communication systems, packet losses could be induced by issues such as propagation phenomena or topological changes [55]. In this sense, ideally, MBPs should overcome such issues and disseminate data through alternative paths. Thus, measuring the lengths of the burst losses allow us to compare the efficiency of different MBPs to overcome the topological changes in the evaluated scenario. To calculate the BAL_i metric for the i-th UAV, a received packet register, $RPreg_{\mathrm{i}}$, is generated during each trial. The k-th position of $RPreg_{\mathrm{i}}$ is set to ''1'' if the SI packet containing $\mathbf{x}^r_k$ is successfully received by the i-th UAV, which is independent of when it was received. Otherwise, if the SI packet containing $\mathbf{x}^r_k$ is lost, the k-th position of $RPreg_{\mathrm{i}}$ is set to ''0''. Then, runs (bursts) of two or more consecutive ''0''s are searched in the list, and the length of each run that is found is stored in a variable B_m. Then, the BAL_i metric is calculated by using:

$$BAL_i = \frac{1}{N_B} \sum\nolimits_{m=1}^{N_B} B_m \tag{25}$$

where B_m is the length of the m-th burst sequence and N_B is total number of bursts that are found in $RPreg_{\mathrm{i}}$. Note that even though two sequences can have the same packet loss, their BAL metric could differ. For example, consider the content of the following registers:

$$RPreg_1 = [0, 0, 1, 1, 0, 0, 1, 1, 0, 0, 1, 1, 0, 0, 1]\,, \tag{26}$$

$$RPreg_2 = [1, 0, 0, 0, 0, 1, 1, 1, 0, 0, 0, 0, 1, 1, 1]\,. \tag{27}$$

Note that $\mathrm{BAL}_1 = 2$ and $\mathrm{BAL}_2 = 4$, even though the packet loss is the same for both UAVs.

The trajectory and network metrics previously introduced are used in Section VI to study and evaluate the performance of MBPs when they are used for SI dissemination. Furthermore, in Section VI-B, the time moving averages of these metrics are calculated, which is done in order to analyze the evolution of the metrics as the UAV formation follows the reference trajectory. The time moving average metrics are calculated by considering an averaging sliding window of 10 consecutive controller samples. To obtain a plot, the averaging sliding window is displaced by a controller sampling period, t_c, each time. The sliding window of 10 samples is enough to capture the network interactions occurring within the reachable radio range of each UAV. Hereafter, these metrics are called metrics by segments.

C. DESIGN AND IMPLEMENTATION OF THE EVALUATION FRAMEWORK

The evaluation methodology was implemented by developing an evaluation framework based on the well-known OMNeT++ network modeler [48], MATLAB®, and the ACADO toolkit [49]. The following subsections elaborate on the design and implementation details of the evaluation framework, which can be made available to the interested reader upon request.

The designed evaluation framework considers three main building blocks (see Fig. 9): 1) a reference trajectory generator, 2) a mobility controller API, and 3) a FANET simulator implemented in OMNeT++. The reference trajectory generator works offline, and the mobility controller API is used by the FANET simulator to determine the flight parameters of each follower UAV, as explained next.

1) REFERENCE TRAJECTORY GENERATOR

To generate and use the trajectory defined in subsection V-A-3 within the evaluation framework, a reference trajectory generator was designed and implemented using MATLAB® and the ACADO toolkit. It is worth noting that defining the UAV trajectories for evaluation purposes is not a simple task since the trajectories must satisfy the restrictions imposed by the UAVs kinematic model.

The reference trajectory generator works offline from the FANET simulator (implemented in OMNeT++). Thus, a valid reference trajectory for virtual point tracking must be generated before starting a simulation trial. The process to generate the trajectory is as follows:

a) A reduced set of milestones are defined by considering the kinematic model of the UAV explained in subsection III-A-1 and the values provided in Table 2. These milestones are delivered to the ACADO toolkit through the MATLAB® interface.
b) The ACADO toolkit returns the reference trajectory, which includes the set of points corresponding to the intermediate points between each pair of milestones and the milestones themselves. The sampling period of the controller directly determines the number of intermediate points between milestones.
c) The valid trajectory that is returned by the ACADO toolkit is formatted in MATLAB® for compatibility with the FANET simulator, which is based on the OMNeT++ network modeler.

Once a valid trajectory is generated, it is feed to the FANET simulator where it will be used by the source/leader UAV to disseminate the SI that is needed for virtual point tracking.

Note that with the reference trajectory generator, any valid trajectory can be easily adjusted to different controller sampling periods and formatted for the OMNeT++ network modeler. In fact, with small variations in the template, the trajectory could be formatted to be used with other network modelers such as NS-2.

2) MOBILITY CONTROLLER

A mobility controller API to solve the nonlinear MPC equations that are required to determine the flying parameters (e.g., speed and roll angle) of each follower UAV was programmed and included in the FANET simulator. At each sampling time step, the API is used to solve the MPC equations on the fly for each UAV within the formation (see subsection III-A-2). The generated API is based on the MPC controller of the ACADO toolkit.

3) FANET SIMULATOR

The FANET simulator is the core module of the implementation framework and is based on the OMNeT++ network modeler [48]. The simulator integrates the mobility controller API and the trajectory generator modules.

The FANET simulator allows modeling the delay and packet loss behavior that are observed when a particular MBP is used for SI dissemination within a FANET. Thus, the MBPs described in subsection III-B-1 were implemented in the simulator such that they can be used to disseminate the SI corresponding to the virtual point trajectory. It is important to recall that the SI messages originate from the source/leader UAV while the rest of the UAVs within the formation have no prior information regarding the mission trajectory. Being based in OMNeT++, the FANET simulator provides the tools that are necessary to obtain common network performance statistics, as explained in subsection V-B-2.

TABLE 3. MBP parameters in the evaluation scenario.

MBP	Parameters
Simple Flooding	-
DTh-Distance-Based	$\{D = 135$ m, $RT \in \mathbb{N} \in [1,10]$ ms $\}$
WT-Distance-Based	$\{MaxWT = 10$ ms $\}$
Probabilistic-Based	$\{WT = 5$ ms, $\delta = 5$ ms $\}$
C-Counter-Based	$\{C = 3, RT \in \mathbb{N} \in [1,10]$ ms $\}$

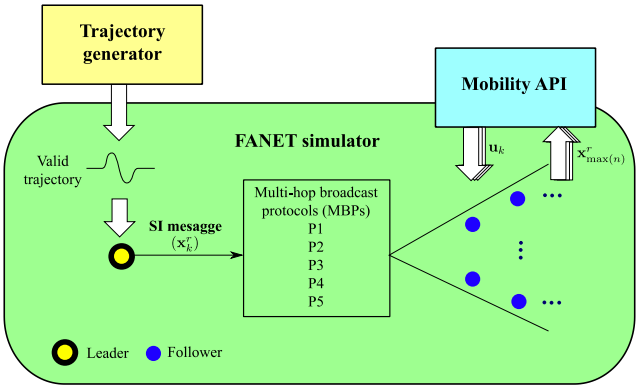

FIGURE 9. Proposed implementation framework.

The particular parameters used for each of the MBPs evaluated in this work are provided in Table 3. These parameters were taken from [35] for Simple flooding, [36] for DTh-Distance-Based, [35] for WT-Distance-Based, [37] for Probabilistic-Based, and [36] for C-Counter-Based. These values were chosen to avoid any bias in the evaluation.

Fig. 9 depicts the interaction between the modules detailed in subsections V-C-1, V-C-2, and V-C-3 during a simulation run. As it can be seen in this figure, the virtual point trajectory is uploaded to the source/leader UAV before the simulation starts. A warm-up period corresponding to a straight-line of 1000 m is considered at the beginning of every simulation trial. Then, in each SI dissemination period, t_d, the source/leader UAV generates the SI message containing the SI vector, $\mathbf{x}_n^r$, which will be disseminated to all UAVs within the formation by means of a particular MBP. In each controller sampling period, t_c, the mobility controller API is used to calculate the actuator control vector, $\mathbf{u}_k$, of each UAV based on its current estate vector, $\mathbf{x}_k$, and the latest SI, $\mathbf{x}_{max(n)}^r$, successfully received.

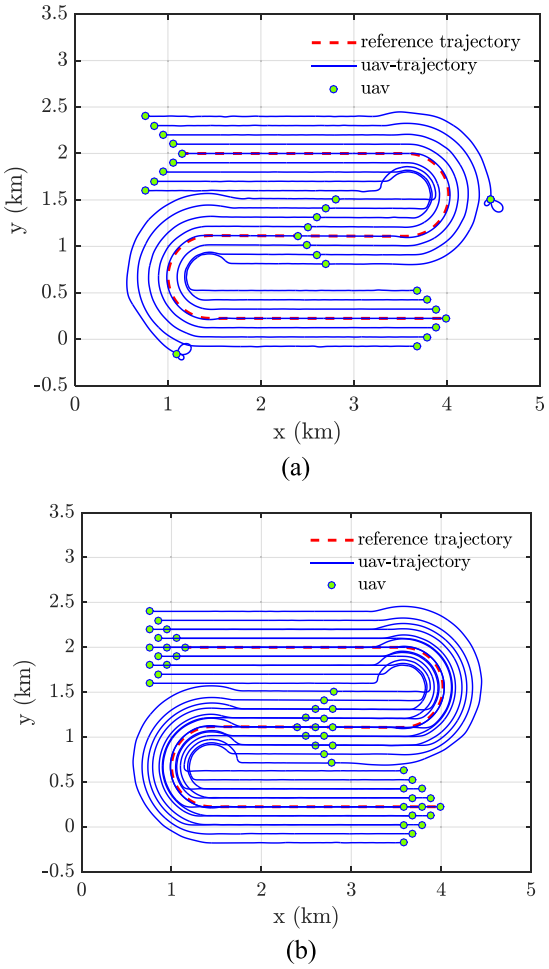

FIGURE 10. Examples of the UAV trajectories that are obtained when using Simple Flooding for SI dissemination in (a) open-delta and (b) delta formations. The sweep trajectory shown in Fig. 6 with a reference speed of $v_r = 25$m/s was assumed. The open-delta formation size was set to $\lambda = 9$, and the delta formation size was set to $\lambda = 15$.

To evaluate the performance of a particular MBP, the metrics described in subsection V-B are calculated at the end of each simulation trial. Additionally, the results of a minimum of 2000 trials are averaged to achieve statistical significance. Furthermore, all metrics that are presented in the following section were obtained by considering that $t_d = t_c = 0.5$ s and a packet size of 512 bytes.

Note that because of the modular design of the FANET simulator, MBPs different from those described in subsection III-B can be readily implemented.

VI. PERFORMANCE RESULTS AND ANALYSIS OF MBPS

This section introduces the results obtained using the evaluation framework and methodology proposed in the previous section.

Flight formation determines the network topology. Thus, it is one of the most relevant factors to consider in the evaluation. To illustrate this, Fig. 10 shows a single simulation run for an open-delta formation with $\lambda = 9$ and a delta formation with $\lambda = 15$. The sweep trajectory shown in Fig. 10 was used with a reference speed of $v_r = 25\ m/s$. The SI messages were generated by the leader UAV every 500 ms and were disseminated using Simple Flooding.

As can be readily seen in Fig. 10, the number of paths through which SI messages can reach UAVs in the last level of each formation can be very different for the open-delta and delta formations. This could lead to significant differences in the MBP performance evaluations. In addition, note in Fig. 10 that two UAVs are lost when flying in open-delta formation, whereas none are lost when flying in delta formation. However, this result does not imply that for a delta formation with $v_r = 25\ m/s$ and $\lambda = 15$, Simple Flooding will enable the proper functioning of the UAV formation control strategy since Fig. 10 only shows the results of a single simulation run. Thus, an extended analysis of how the performance of the MBPs affects the distributed UAV formation control strategy is provided next.

A. OVERALL RESULTS

This subsection presents the performance evaluation of the MBPs under study considering open-delta and delta formations, two formation sizes, and different reference speeds for the mission. The metrics used for the evaluation are the P-RMSE, LU, PDR and $\text{AvgSIage}_{\text{L}_\text{m}}$ that were introduced in Section V.

Fig. 11 and Fig. 12 show the P-RMSE and LU results obtained for the MBPs under evaluation for the open-delta formation and different reference speeds. In addition, Fig. 11 shows the P-RMSE for the ideal protocol, i.e., all SI messages arrive on time to every UAV in the flight formation. In these figures, it can be seen that both the P-RMSE and the LU increase as the reference speed increases, especially from 22.5 m/s to 27.5 m/s. Some of this behavior can be attributed to factors related to the controller and the UAV flight dynamics since in the ideal case (red line) the P-RMSE increases with the speed as well. However, note how there are no lost UAVs in the ideal case, while when using MBPs, the LU metric increases significantly for 25 m/s and 27.5 m/s.

By closely examining Fig. 11 and Fig. 12, the following observations can be made:

- The P-RMSE and LU metrics are worse for the largest formation size. This is expected, because as the formation size increases, the number of hops needed to reach the UAVs that are located at the edge increases as well.
- In general, the worst performance is offered by the WT-Distance-Based protocol.
- Overall, for the high reference speeds (25 m/s and 27.5 m/s), the trajectory performances offered by the 135Th-Distance-Based and the 3-Counter-Based MBPs are better than the others.
- Simple Flooding seems to work well for low and medium speeds; however, as the speed increases, its trajectory performance worsens.

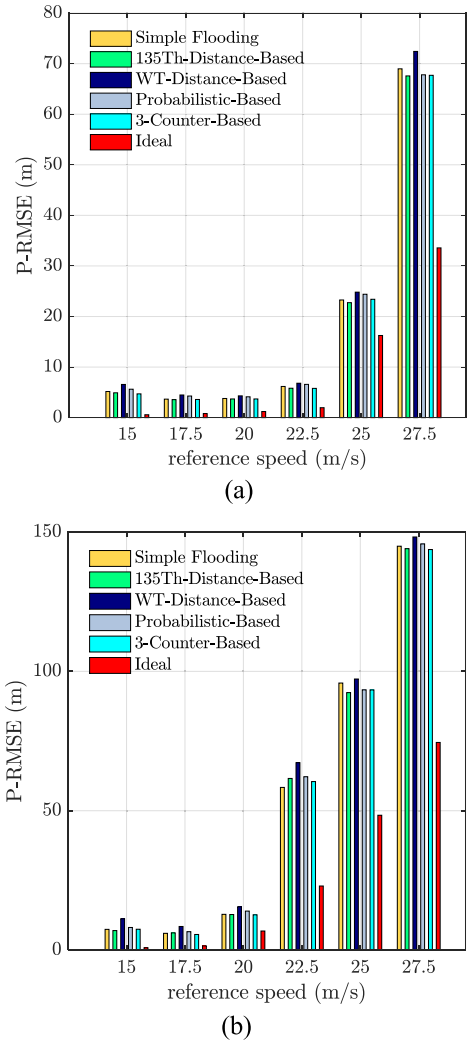

FIGURE 11. P-RMSE obtained with different MBPs in a UAV mission using the open-delta formation with (a) $\lambda = 7$ and (b)$\lambda = 9$. The reference speed varies from $v_r = 15$ to $v_r = 27.5$ m/s. The results were obtained by averaging a minimum of 2000 runs to achieve statistical significance.

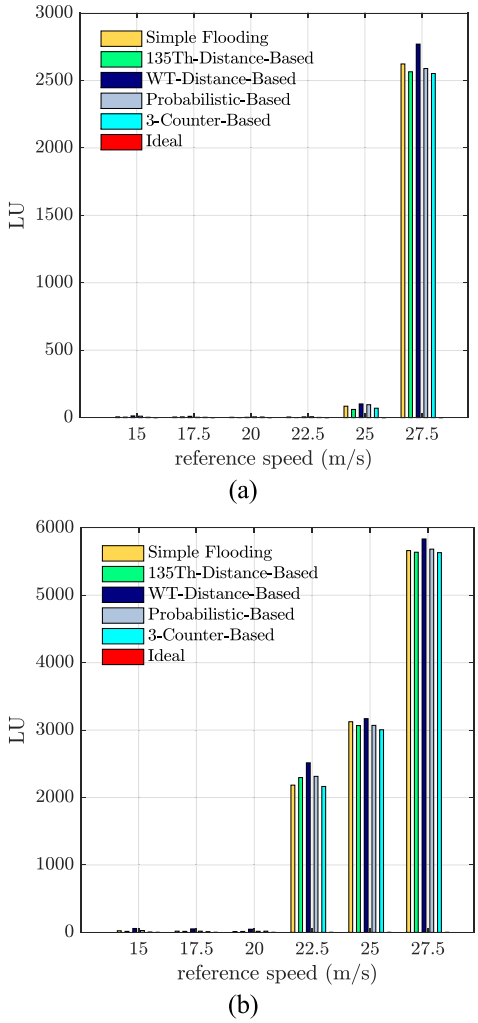

FIGURE 12. LU (lost UAVs) metric obtained with different MBPs in a UAV mission using the open-delta formation with (a) $\lambda = 7$ and (b)$\lambda = 9$. The reference speed varies from $v_r = 15$ to $v_r = 27.5$ m/s. The results were obtained by averaging a minimum of 2000 runs to achieve statistical significance.

The average PDR and $\text{AvgSIage}_{\text{L}_\text{m}}$ for this setup are presented in Fig. 13, Fig. 14, and Fig. 15. Only plots of $\text{AvgSIage}_{\text{L}_\text{m}}$ for the last two formation levels are provided in Fig. 14 ($\lambda = 7$) and Fig. 15 ($\lambda = 9$). The following observations can be made from these figures:

- The PDR and $\text{AvgSIage}_{\text{L}_\text{m}}$ are worse for $\lambda = 9$ (the largest formation size).
- For both $\lambda = 7$ and $\lambda = 9$, the WT-Distance-Based MBP provides the worst performance (the lowest PDR and highest $\text{AvgSIage}_{\text{L}_\text{m}}$).
- Simple Flooding provides a PDR and $\text{AvgSIage}_{\text{L}_\text{m}}$ that seem to be close to the best among the MBPs.
- The 135Th-Distance-Based and the 3-Counter-Based MBPs provide the best overall network performance.
- It seems that when the PDR is below 0.7 and the $\text{AvgSIage}_{\text{L}_\text{m}}$ is above 1, the LU metric increases significantly for all MBPs.

By analyzing the results presented in Figs. 11 to 15, it can be observed that, in general, there is a good correspondence between the trajectory performance metrics and the network performance metrics. That is, the MBPs that provide better network performance provide better trajectory performance for the open-delta formation. Particularly, the 135Th-Distance-Based and the 3-Counter-Based MBPs exhibited the best trajectory and network performances overall. Note that these protocols use a random waiting time before a rebroadcast attempt, and the probability of canceling a packet rebroadcast is low for the evaluation scenario that is considered. Also, observe that Simple Flooding does not provide the worst performance. Thus, the results allow to infer that the best option for open-delta formations is to use MBPs where: a) the probability of canceling packet rebroadcasts is low (but not necessarily equal to zero as in Simple Flooding); b) the PDR is high and the $\text{AvgSIage}_{\text{L}_\text{m}}$ is low.

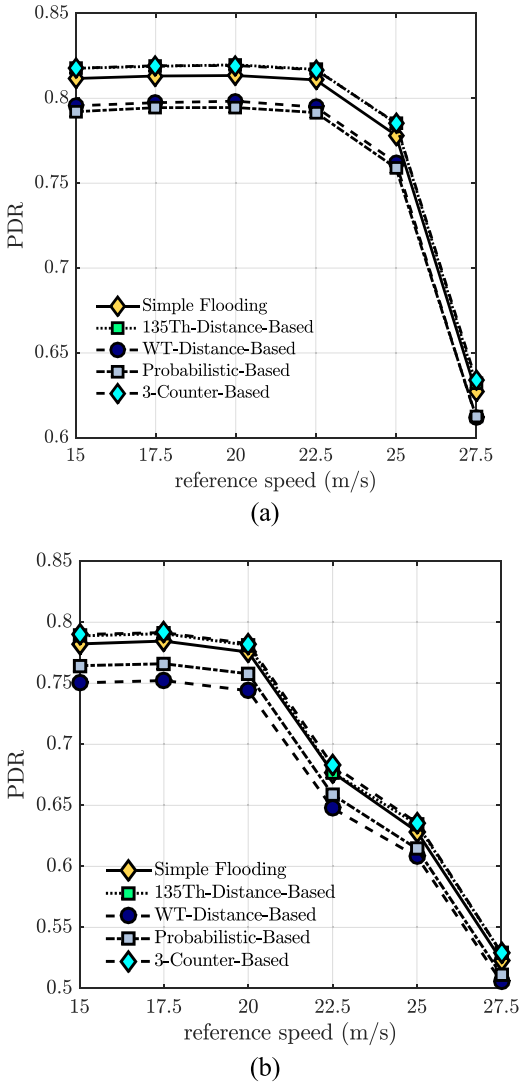

FIGURE 13. PDR obtained with different MBPs in a UAV mission using the open-delta formation with (a) $\lambda = 7$ and (b)$\lambda = 9$. The reference speed varies from $v_r = 15$ to $v_r = 27.5$ m/s. The results were obtained by averaging a minimum of 2000 runs to achieve statistical significance.

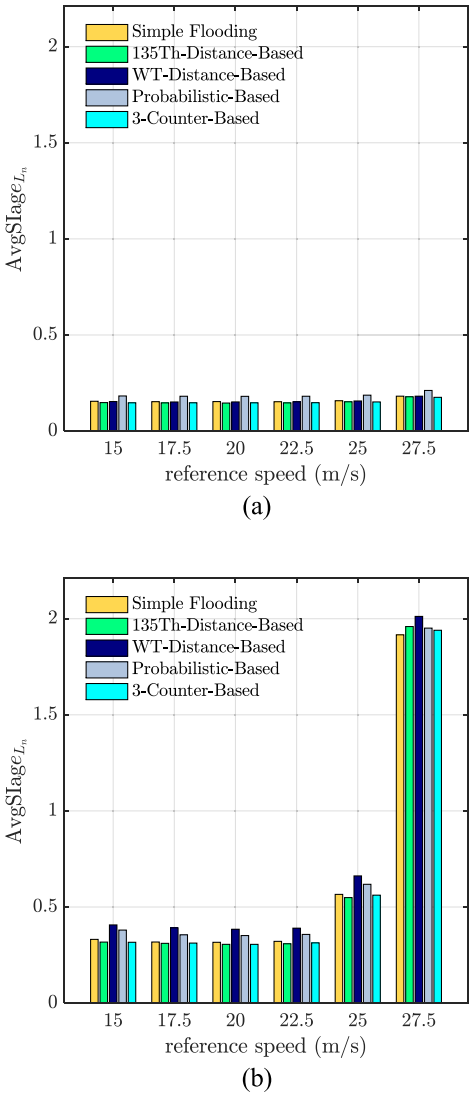

FIGURE 14. AvgSIage_{L_m} obtained with different MBPs in a UAV mission using the open-delta formation with $\lambda = 7$ for (a)L_3 and (b)L_4. The reference speed varies from $v_r = 15$ to $v_r = 27.5$ m/s. The results were obtained by averaging a minimum of 2000 runs to achieve statistical significance.

Continuing with the analysis of the results provided in Figs. 11 to 15, note that at high speeds the trajectory and network metrics do not show the same tendencies for the WT-Distance-Based, the Simple Flooding, and the Probabilistic-Based MBPs. For example, for $\lambda = 7$ and $v_r = 27.5$ m/s, the protocols with the worst trajectory metrics are WT-Distance-Based and Simple Flooding. However, for these values, the protocols providing the worst network metrics are the WT-Distance-Based followed by the Probabilistic-Based. In this sense, note that when the formation enters and leaves a turn, the network topology could change. Thus, in order to explain this behavior, an in-deep analysis of the evolution of the metrics through the trajectory is provided in subsection VI-B.

Fig. 16 and Fig. 17 show the P-RMSE and LU results obtained for the MBPs under evaluation for the delta formation and different reference speeds. In these figures, it can be seen that both the P-RMSE and LU increase as the reference speed increases (particularly from 25 m/s to 27.5 m/s). As in the open-delta formation, some of this behavior can be attributed to factors related to the controller and the UAV flight dynamics. Similar to the open-delta formation, there are no lost UAVs in the ideal case. However, when using MBPs, the LU metric increases significantly for 25 m/s and 27.5 m/s (especially for the largest formation size). Nevertheless, note that the trajectory metrics obtained for the delta formation are better than those obtained for the open-delta formation.

By closely examining Fig. 16 and Fig. 17, the following observations can be made:

- Overall, the worst performance is obtained when using the WT-Distance-Based protocol (as with the open-delta formation).

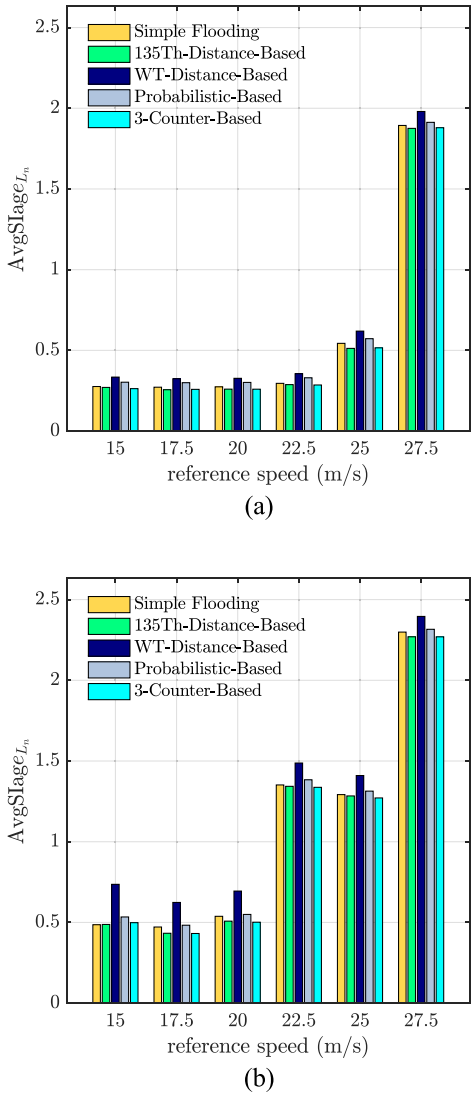

FIGURE 15. **AvgSIage$_{L_m}$ obtained with different MBPs in a UAV mission using the open-delta formation with $\lambda = 9$ for (a)L_4 and (b)L_5. The reference speed varies from $v_r = 15$ to $v_r = 27.5$ m/s. The results were obtained by averaging a minimum of 2000 runs to achieve statistical significance.**

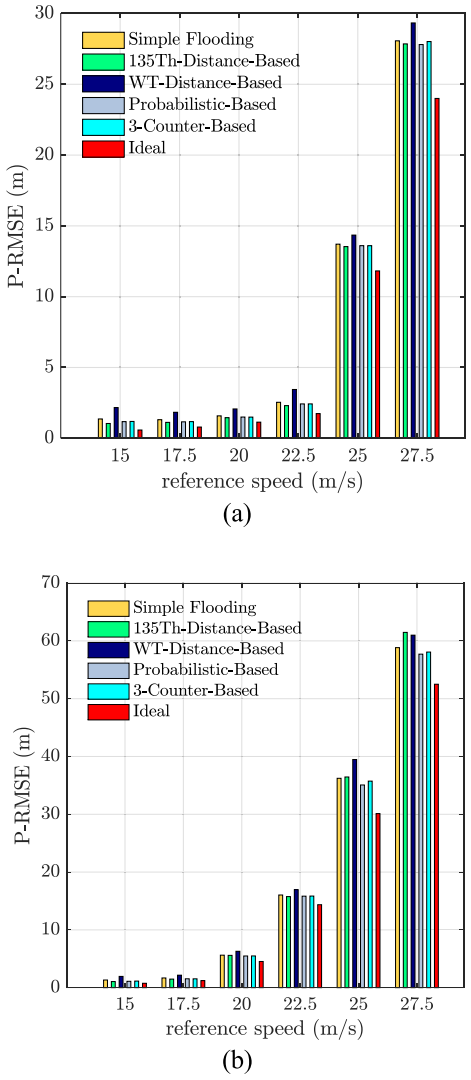

FIGURE 16. **P-RMSE obtained with different MBPs in a UAV mission using the delta formation with (a) $\lambda = 10$ and (b)$\lambda = 15$. The reference speed varies from $v_r = 15$ to $v_r = 27.5$ m/s. The results were obtained by averaging a minimum of 2000 runs to achieve statistical significance.**

- For low (15 m/s and 17.5 m/s) to medium (20 m/s and 22.5 m/s) reference speeds, the performance of all MBPs is similar, except for the WT-Distance-Based protocol.
- The P-RMSE and LU metrics are the worst for larger formation sizes, as expected.
- The 135Th-Distance-Based protocol seems to work well for $\lambda = 10$ at low and medium speeds. However, as the speed increases to 27.5 m/s, its performance worsens (see the LU metric in Fig. 14).
- For $\lambda = 15$, the performance drop exhibited by 135Th-Distance-Based as the speed increases is notorious. Furthermore, its performance at 27.5 m/s is even worse than that provided by WT-Distance-Based.
- The Probabilistic-Based protocol seems to provide the best trajectory performance overall.
- The P-RMSE and LU metrics are better for the delta formation than for the open-delta formation.

The average PDR and AvgSIage$_{L_m}$ for this setup are presented in Fig. 18, Fig. 19, and Fig. 20. Only plots of AvgSIage$_{L_m}$ for the last two formation levels are provided in Fig. 19 ($\lambda = 10$) and Fig. 20 ($\lambda = 15$). The following observations can be made from these figures:

- For both formation sizes ($\lambda = 10$ and $\lambda = 15$), WT-Distance-Based exhibits the worst performance (lowest PDR and higher AvgSIage$_{L_m}$).
- For low (15 m/s and 17.5 m/s) to medium (20 m/s and 22.5 m/s) reference speeds, the 135Th-Distance-Based and the Probabilistic-Based MBPs exhibit the best PDR and AvgSIage$_{L_m}$ metrics.
- For high reference speeds (25 m/s and 27.5 m/s), the network performance of 135Th-Distance-Based worsens.

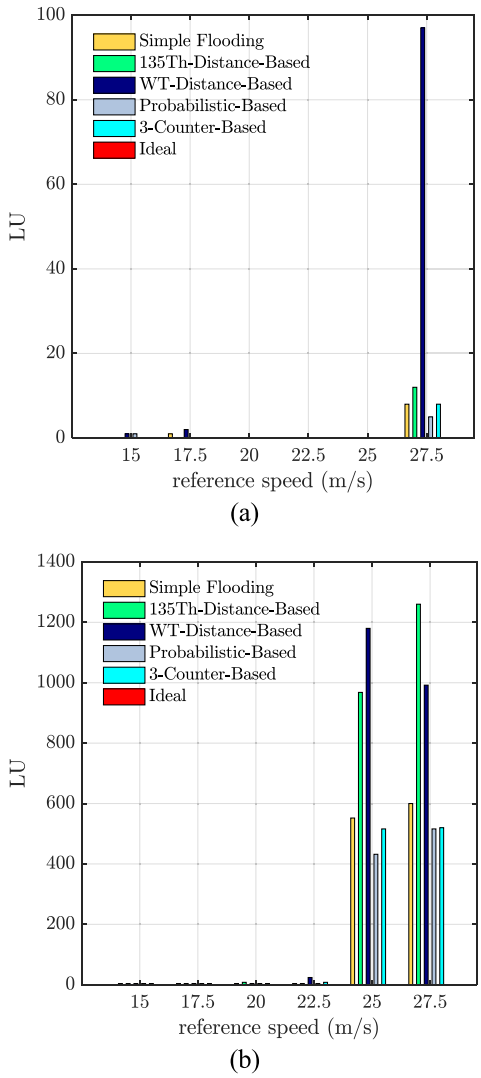

FIGURE 17. LU (lost UAVs) metric obtained with different MBPs in a UAV mission using the delta formation with (a) $\lambda = 10$ and (b)$\lambda = 15$. The reference speed varies from $v_r = 15$ to $v_r = 27.5$ m/s. The results were obtained by averaging a minimum of 2000 runs to achieve statistical significance.

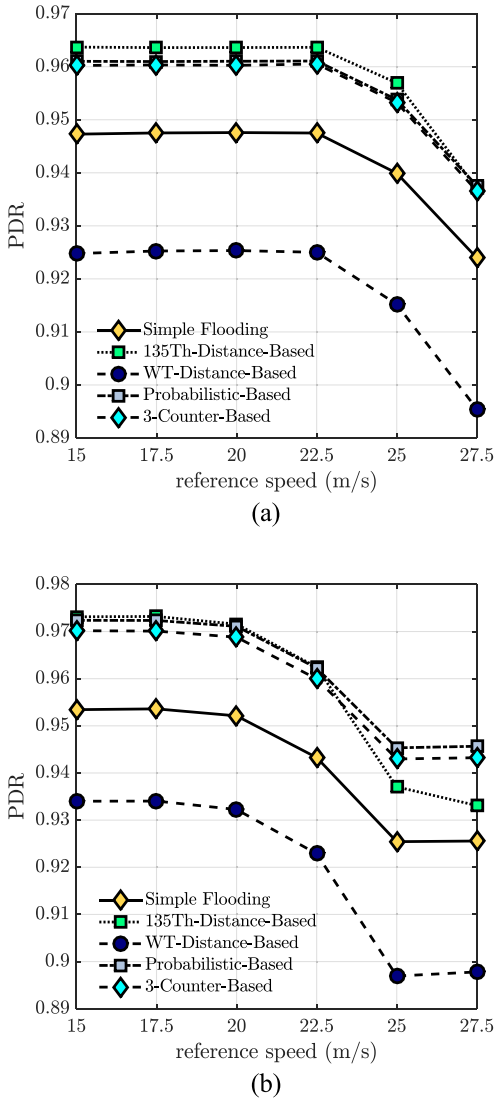

FIGURE 18. PDR obtained with different MBPs in a UAV mission using the delta formation with (a) $\lambda = 10$ and (b)$\lambda = 15$. The reference speed varies from $v_r = 15$ to $v_r = 27.5$ m/s. The results were obtained by averaging a minimum of 2000 runs to achieve statistical significance.

The performance decrease is particularly sharp for the larger $\lambda = 15$.

- In contrast, for high reference speeds (25 m/s and 27.5 m/s) and $\lambda = 15$, the Probabilistic-Based MBP exhibits the best network performance.

By analyzing the results presented in Figs. 16 to 20, it can be observed that, as with the open-delta formation, in general, there is a good correspondence between the trajectory performance metrics and the network performance metrics. However, there are significant differences in the performance offered by different MBPs when the UAVs fly in delta formation compared to the performance observed for the open-delta formation. In particular, the Probabilistic-Based protocol seems to provide the best trajectory performance overall for the delta formation, which is not the case for the open-delta formation. In this sense, note that, compared to the open-delta formation, the delta formation is a denser network where each node has at least two neighbors at the beginning of the flight mission. This is an important observation since MBPs are usually designed to work over dense scenarios, such as those found in VANETs deployments. In particular, it is commonly assumed that denser networks are more challenging for MBPs. Thus, at first sight, the obtained results seem to be counterintuitive. However, it should be noted that, when compared with common ad-hoc scenarios, delta and open-delta formations are low-density scenarios. Therefore, in the evaluation scenario, the obtained results should be analyzed while considering connectivity issues. In this sense, UAVs flying in a delta formation will have higher connectivity compared to UAVs flying in an open-delta formation. This means that a UAV flying in a delta formation has more nodes

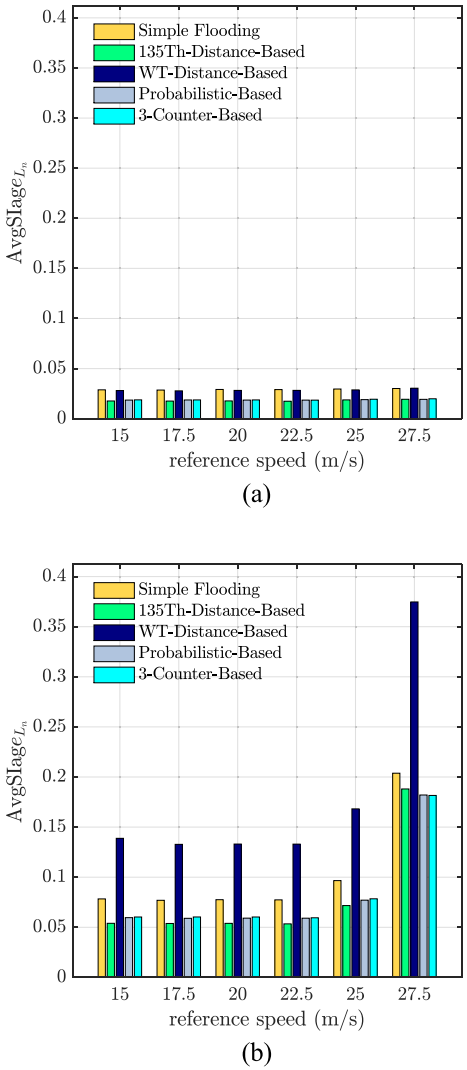

FIGURE 19. **AvgSIage$_{L_m}$ obtained with different MBPs in a UAV mission using the delta formation with $\lambda = 10$ for (a)L_3 and (b)L_4. The reference speed varies from $v_r = 15$ to $v_r = 27.5$ m/s. The results were obtained by averaging a minimum of 2000 runs to achieve statistical significance.**

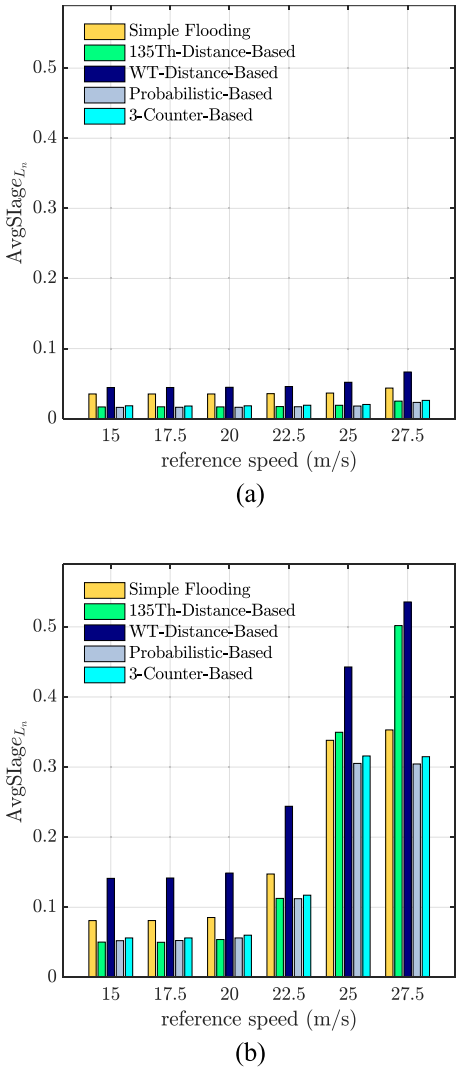

FIGURE 20. **AvgSIage$_{L_m}$ obtained with different MBPs in a UAV mission using the delta formation with $\lambda = 15$ for (a)L_4 and (b)L_5. The reference speed varies from $v_r = 15$ to $v_r = 27.5$ m/s. The results were obtained by averaging a minimum of 2000 runs to achieve statistical significance.**

within reach from which it can receive or relay packets, which in low-density scenarios can lead to improving the PDR but also to more collisions compared to the open-delta formation.

Considering that more collisions can occur in delta formations than in open-delta formations, it is worthwhile to calculate a "collision ratio" (CR) as a metric to compare the cost of the PDR achieved by each MBP under evaluation. In particular, in this paper, the CR is calculated by counting the total number of collisions that occur during a simulation trial and then dividing the result by the total number of packets that are sent by the leader UAV. Fig. 21 shows the CR obtained for the different MBPs under evaluation for the delta formation. Note that WT-Distance-Based has the lowest CR followed by Probabilistic-Based. However, the WT-Distance-Based has the lowest PDR, which helps to explain why the trajectory performance offered by the Probabilistic-Based MBP is better. Furthermore, by observing Figs. 18 to 21, it can be concluded that the Probabilistic-Based MBP offers a better tradeoff between the PDR, AvgSIage$_{L_m}$, and CR compared to the other MBPs under evaluation, particularly for high speeds and $\lambda = 15$. This, in turn, translates to better trajectory performance, as observed in Fig. 16 and Fig. 17.

Although the previous analysis may help to explain why the Probabilistic-Based MBP provides the best trajectory metrics at high speeds, no conclusion can be made about why the 135Th-Distance-Based MBP shows the performance drop at high speeds (25 m/s and 27.5 m/s). In that sense, it is worth recalling that, except for Simple Flooding, all protocols under evaluation include mechanisms that cancel packet retransmissions when a certain criterion is fulfilled. Therefore, in addition to collisions, a distant node might not receive an SI packet because of a rebroadcast cancellation. However, for the proper functioning of the formation control strategy, it is necessary to periodically receive the

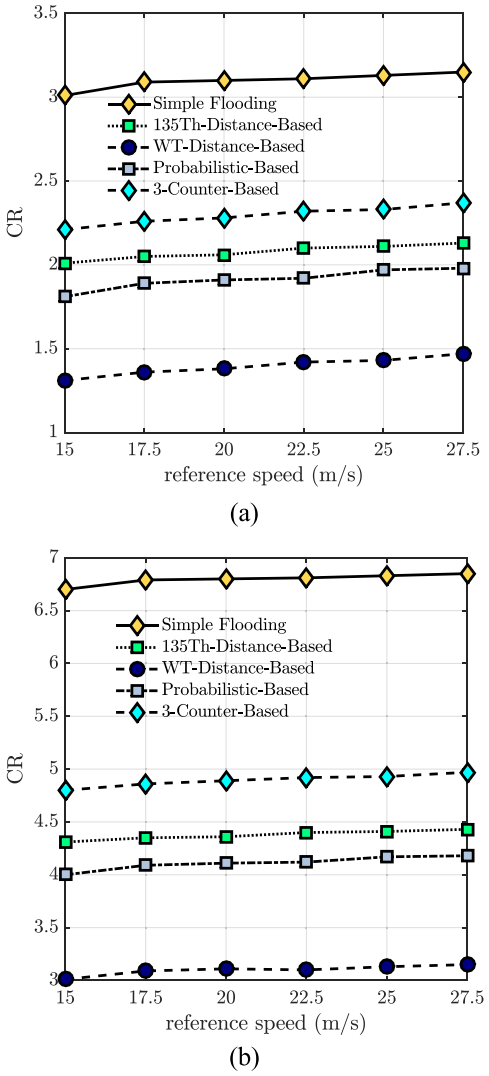

FIGURE 21. Collision ratio (CR) obtained with different MBPs in a UAV mission using the delta formation with (a) $\lambda = 10$ and (b)$\lambda = 15$. The reference speed varies from $v_r = 15$ to $v_r = 27.5$ m/s. The results were obtained by averaging a minimum of 2000 runs to achieve statistical significance. The CR is calculated by counting the total number of collisions that occurred during the simulation and dividing that by the total number of source packets that are sent by the leader UAV.

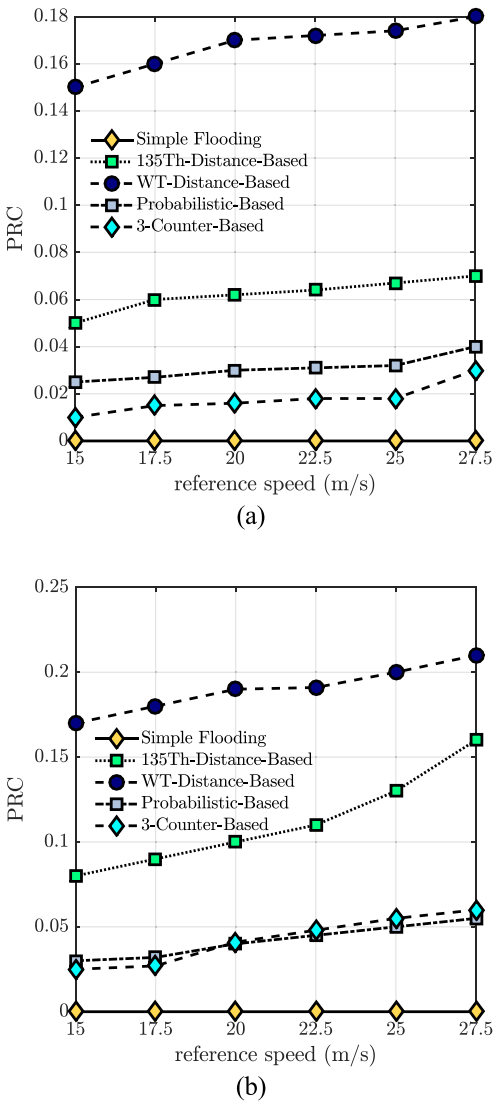

FIGURE 22. Percentage of packet rebroadcasts that are canceled (PRC) obtained with different MBPs in a UAV mission using the delta formation with (a) $\lambda = 10$ and (b)$\lambda = 15$. The reference speed varies from $v_r = 15$ to $v_r = 27.5$ m/s. The results were obtained by averaging a minimum of 2000 runs to achieve statistical significance. The PRC is calculated by measuring the average percentage of packets rebroadcasts that are canceled during the simulation.

SI that is generated by the leader UAV. Thus, it is worthwhile to calculate the percentage of packet rebroadcasts that are canceled (PRC) by each MBP under evaluation. The PRC is shown in Fig. 22. Note how WT-Distance-Based cancels more packet rebroadcasts for this scenario than the other MBPs. This further explains why WT-Distance-Based exhibits the worst trajectory metrics. Nevertheless, note how the second MBP that cancels more rebroadcasts is 135Th-Distance-Based. This helps to explain why at high speeds this protocol has a significant performance drop, especially for $\lambda = 15$.

The PRC plot helps to explain the trajectory performance drop that is observed when using the 135Th-Distance-Based MBP for $\lambda = 15$. However, the trajectory performance exhibited by 135Th-Distance-Based is even worse for $v_r = 27.5$ than that obtained when using WT-Distance-Based (see Fig. 17(b)). Therefore, to gain more insight into this behavior, an in-deep analysis of the evolution of the metrics through the trajectory is provided in subsection VI-B.

B. RESULTS BY SEGMENTS

In this section, an analysis considering the time evolution of the evaluation metrics is presented. Specifically, the sweep trajectory considered in the previous sections was divided into seven segments, as shown in Fig. 23.

This analysis aims to track the evolution of the network metrics as the UAV formation follows the reference trajectory.

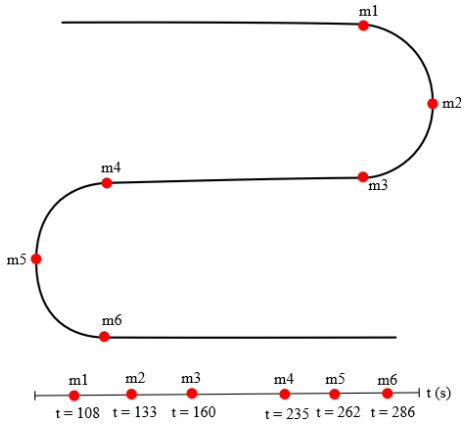

FIGURE 23. Reference trajectory considering its segments.

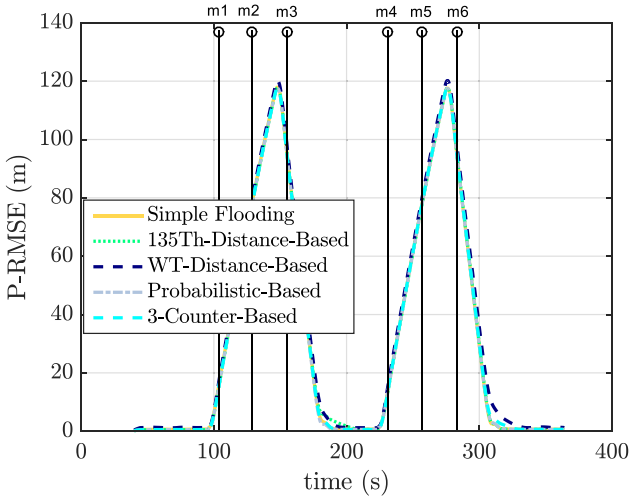

FIGURE 24. Moving average P-RMSE obtained when SI messages are disseminated with the different MBPs considered. For this figure, UAVs fly in delta formation with a reference speed = 27.5 m/s and $\lambda = 10$. The results at each sampling period were obtained using the average of a minimum of 2000 runs to achieve statistical significance. Only the UAVs from the third level or higher were considered for this figure.

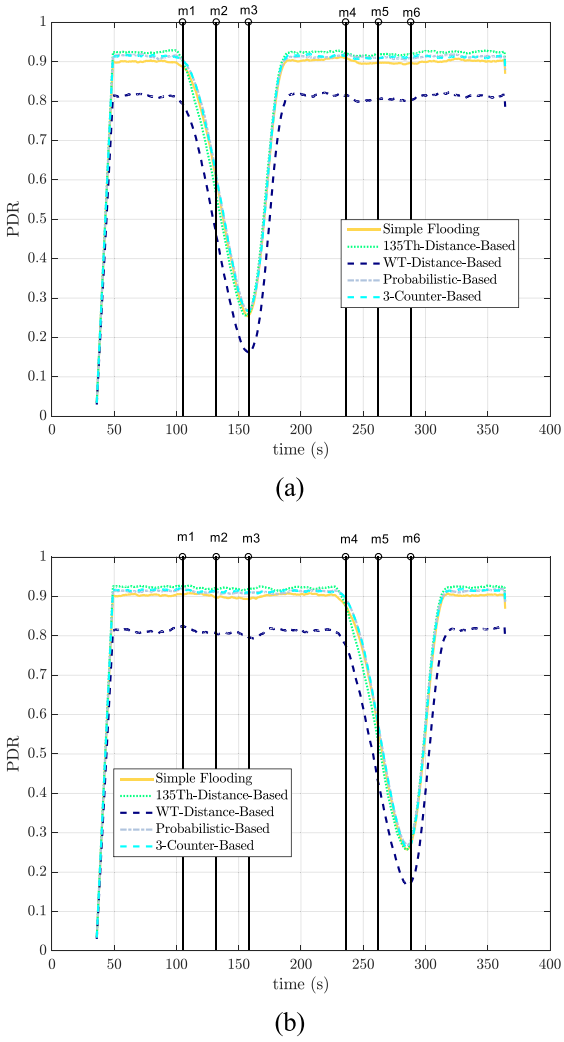

FIGURE 25. Moving average PDR obtained when SI messages are disseminated with the different MBPs considered. For this figure, UAVs fly in delta formation with a reference speed = 27.5 m/s and $\lambda = 10$. Only the UAVs that are located at the (a) south-west (UAV7) and (b) south-east (UAV10) edges of the formation were considered for the calculations. The results at each sampling period were obtained using the average of a minimum of 2000 runs to achieve statistical significance.

To this end, the network metrics were calculated using a moving average of 10 sample periods. In this way, fast fluctuations in the performance metrics are smoothed, and good insights into the evolution of the metrics can be achieved. In addition to the network metrics used in the previous section, the burst average length (BAL) of the losses (see subsection V-B-2) is considered in the analysis.

Fig. 24 shows the moving average P-RMSE obtained for the different MBPs under evaluation for the delta formation with $\lambda = 10$ and $v_r = 27.5$ m/s. For this figure, only the UAVs from the third level or higher were considered for the P-RMSE calculation. The P-RMSE is presented considering the segments shown in Fig. 23. It can be seen in Fig. 24 that, in general, the moving average P-RMSE of all MBPs increases as the UAVs make the turn (segments $m_1{-}m_2 - m_3$ and $m_4{-}m_5 - m_6$) and decreases when UAVs exit from it.

Note that the P-RMSE behavior observed in Fig. 24 agrees with the results of Fig. 16(a) in the sense that the WT-Distance-Based MPB provides a slightly worse P-RMSE performance than the other MBPs. However, note that the behavior observed in the moving average P-RMSE does not fully explain the LU metric results shown in Fig. 17(a) where the performance of WT-Distance-Based is significantly worse than the rest. The reason for this is because once a UAV is definitively lost, it is no longer considered for the P-RMSE calculation.

Furthermore, considering the wireless propagation phenomena, it is reasonable to infer that UAVs that are closer to the leader consistently have better probabilities of successful packet reception. Thus, considering these nodes in the metric calculation in scenarios with a low number of UAVs might bias the average. Therefore, the following analysis is focused on UAVs flying at the edges of the last formation level, which

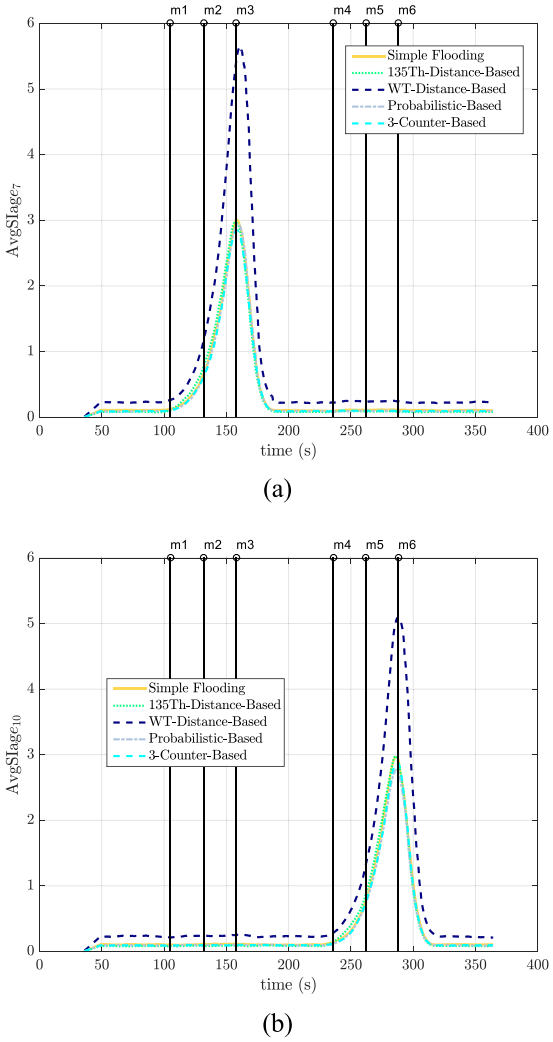

FIGURE 26. Moving average AvgSIage obtained when SI messages are disseminated with the different MBPs considered. For this figure, UAVs fly in delta formation with a reference speed = 27.5 m/s and $\lambda = 10$. Only the UAVs that are located at the (a) south-west (UAV7) and (b) south-east (UAV10) edges of the formation were considered for the calculations. The results at each sampling period were obtained using the average of a minimum of 2000 runs to achieve statistical significance.

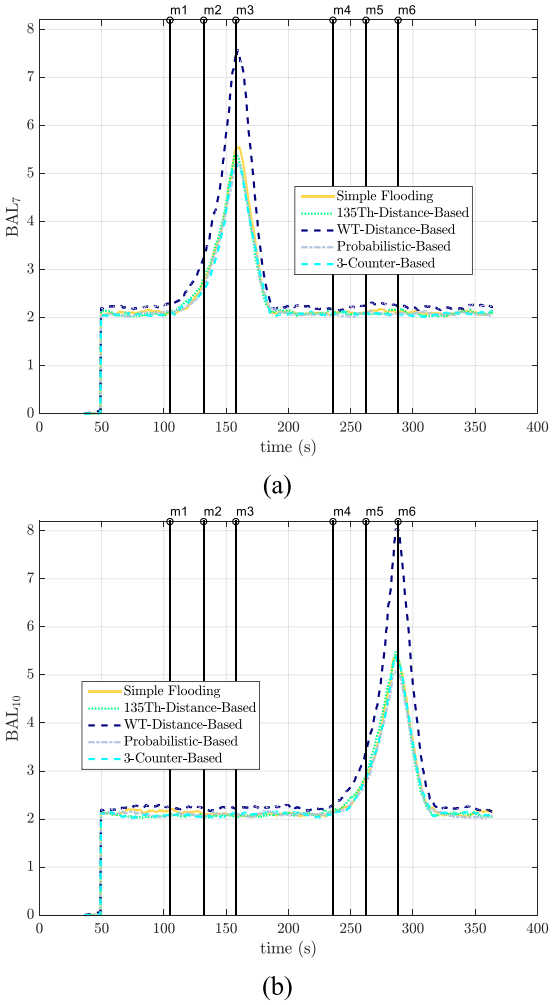

FIGURE 27. Moving average burst average length (BAL) obtained when SI messages are disseminated with the different MBPs considered. For this figure, only burst lengths higher than 1 were considered; and UAVs fly in delta formation with a reference speed = 27.5 m/s and $\lambda = 10$. Only the UAVs that are located at the (a) south-west (UAV7) and (b) south-east (UAV10) edges of the formation were considered for the calculations. The results at each sampling period were obtained using the average of a minimum of 2000 runs to achieve statistical significance.

are more prone to experience challenging network conditions, e.g., disconnections, and fewer neighbors.

To further analyze the LU metric behavior observed in Fig. 17(a) for $\lambda = 10$ and $v_r = 27.5$ m/s, the moving average PDR for the UAVs flying at the formation edges is shown in Fig. 25. In particular, Fig. 25(a) shows the moving average PDR of the UAV that is located in the south-west edge of the formation (referred to the rotated coordinate system $X_r O_r Y_r$ shown in Fig. 2) and labeled UAV7. Similarly, Fig. 25(b) shows the moving average PDR of the UAV that is located in the south-east edge of the formation and labeled UAV10.

Note in Fig. 25 how the PDR significantly decays for UAV7 when it makes the first turn ($m_1 - m_2 - m_3$), while for UAV10 the PDR decays when it makes the second turn ($m_4 - m_5 - m_6$). Thus, the PDRs of UAV7 and UAV10 decay when they make a turn and are located at the outside of the curve while following the reference trajectory of Fig. 23. Following the analysis, Fig. 26 and Fig. 27 show the moving average AvgSIage and BAL for UAV7 and UAV10. As with the PDR, both metrics significantly worsen when the corresponding UAV makes a turn and is located at the outside of a curve in the trajectory.

By closely analyzing the moving average PDR, AvgSIage and BAL results provided in Figs. 25 to 27, respectively, the following observations can be made regarding the network performance offered to the UAVs that are located at the formation edges (UAV7 and UAV10):

- The performance of all MBPs is worse at turns.
- The WT-Distance-Based protocol consistently provides the worst network performance. In addition, it is

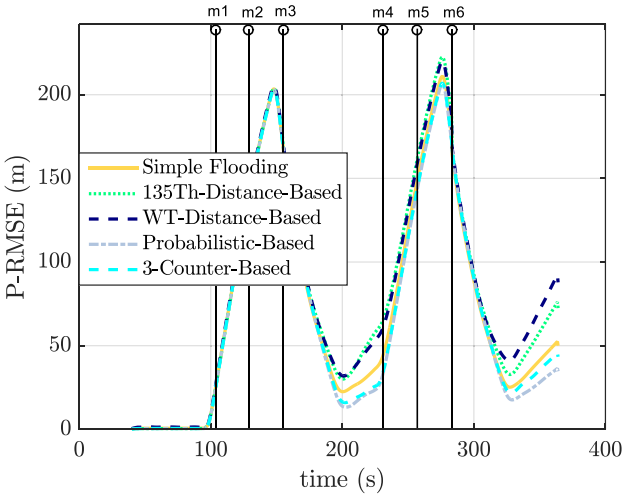

FIGURE 28. Moving average P-RMSE obtained when SI messages are disseminated with the different MBPs considered. For this figure, UAVs fly in delta formation with a reference speed = 27.5 m/s and $\lambda = 15$. The results at each sampling period were obtained using the average of a minimum of 2000 runs to achieve statistical significance.

the MBP that is most affected by network conditions at turns.

- AvgSIage metric indicates that while following a straight-line path, on average, the controller uses recent SI at every sampling time. However, as the formation enters the curve, the AvgSIage increases, which can be caused by significant delays or packet drops. This is particularly acute for the WT-Distance-based protocol since at one point the SI that is used by the controller can be older than 5 sampling periods on average. In contrast, for the other MBPs, the AvgSIage is below 3 sampling periods. This helps to explain why when using WT-Distance-based, more UAVs are lost.
- The BAL metric indicates that when using the WT-Distance-based protocol, the BAL is larger than for the other MBPs.
- By comprehensively analyzing the PDR, AvgSIage and BAL metrics shown in Figs. 25 to 27, respectively, it can be inferred that, in addition to physical link disconnections, the multi-hop broadcast approach of WT-Distance-based induces significant SI dissemination delays and packet losses such that the controller effectiveness at keeping UAV7 and UAV10 within the formation is lost in the curves.

Continuing with the analysis of the results by segments, Fig. 28 shows the moving average P-RMSE obtained for the different MBPs under evaluation for a delta formation with $\lambda = 15$ and $v_r = 27.5$ m/s. For this figure, only the UAVs from the third level or higher where considered for the P-RMSE calculation. The P-RMSE is presented considering the segments shown in Fig. 23. As in Fig. 24, it can be seen in Fig. 28 that the P-RMSE increases as the formation makes a turn and decreases when the formation exits from it. Different from the case with $\lambda = 10$, for $\lambda = 15$, the P-RMSE provided

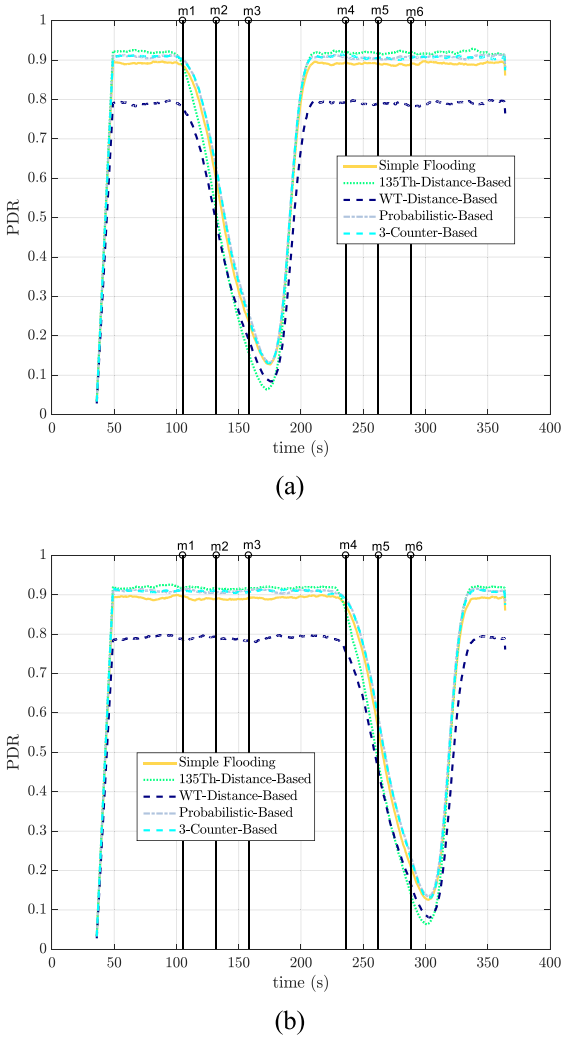

FIGURE 29. Moving average PDR obtained when SI messages are disseminated with the different MBPs considered. For this figure, UAVs fly in delta formation with a reference speed = 27.5 m/s and $\lambda = 15$. Only the UAVs that are located at the (a) south-west (UAV11) and (b) south-east (UAV15) edges of the formation were considered for the calculations. The results at each sampling period were obtained using the average of a minimum of 2000 runs to achieve statistical significance.

by the 135Th-Distance-Based protocol at the turns is slightly worse than that obtained when using the other MBPs.

Continuing with the analysis performed for $\lambda = 15$ and $v_r = 27.5$ m/s, Figs. 29 to 31 show the moving average PDR, AvgSIage, and BAL for UAVs flying at the formation edges for a delta formation with $\lambda = 15$ and $v_r = 27.5$ m/s. For these figures, the network metrics were calculated with a moving average of 10 sample periods. Similar to the previous case, the UAV that is located at the south-west edge of the formation is labeled as UAV11, and the UAV that is flying at the south-east edge of the formation is labeled as UAV15.

Note in Figs. 29 to 31 that, for all MBPs under evaluation, the network performance for UAV11 and UAV15 worsens as the formation makes a turn ($m_1 - m_2 - m_3$ or $m_4 - m_5 - m_6$). However, different from the delta formation with $\lambda = 10$, for

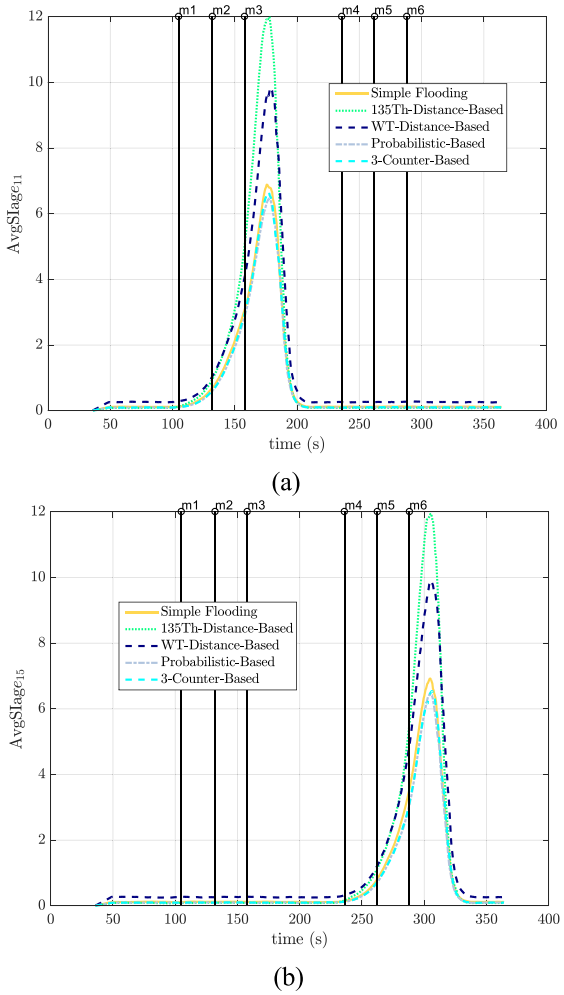

FIGURE 30. Moving average **AvgSIage** obtained when SI messages are disseminated with the different MBPs considered. For this figure, UAVs fly in delta formation with a reference speed = 27.5 m/s and $\lambda = 15$. Only the UAVs that are located at the (a) south-west (UAV11) and (b) south-east (UAV15) edges of the formation were considered for the calculations. The results at each sampling period were obtained using the average of a minimum of 2000 runs to achieve statistical significance.

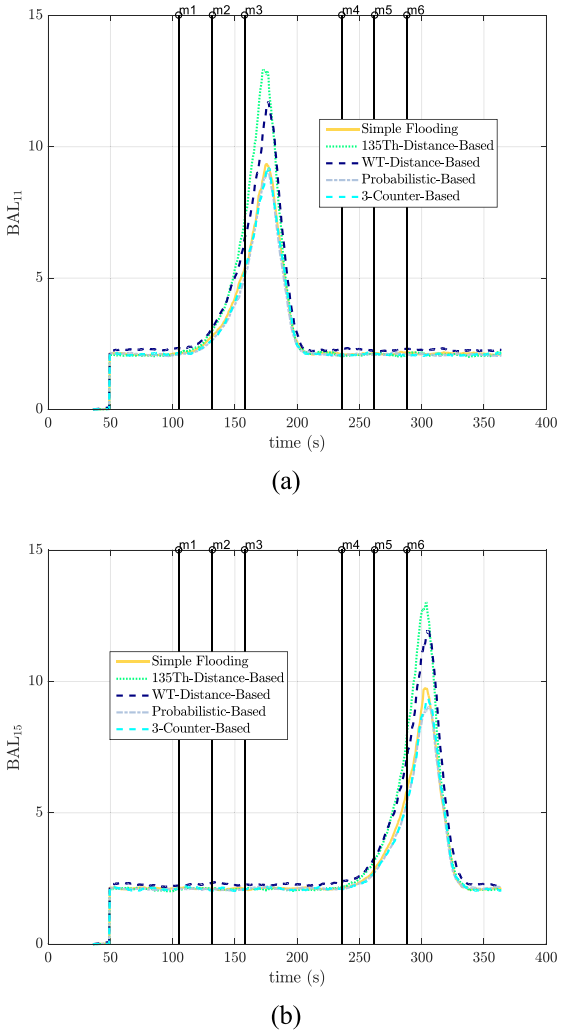

FIGURE 31. Moving average burst average length (BAL) obtained when SI messages are disseminated with the different MBPs considered. For this figure, only burst lengths higher than 1 were considered; and UAVs fly in delta formation with a reference speed = 27.5 m/s and $\lambda = 15$. Only the UAVs that are located at the (a) south-west (UAV11) and (b) south-east (UAV15) edges of the formation were considered for the calculations. The results at each sampling period were obtained using the average of a minimum of 2000 runs to achieve statistical significance.

the case under analysis, the worst performance at the turns is provided by the 135Th-Distance-Based protocol instead of the WT-Distance-Based MBP. This explains the P-RMSE and LU metrics results shown in Fig. 16(b) and Fig. 17(b), respectively, where the 135Th-Distance-Based MBP provides the larger P-RMSE and LU for $\lambda = 15$ and $v_r = 27.5$ m/s.

In summary, for the UAVs that are located at the south-west and south-east edges of a delta formation, the network performance provided by the different MBPs is acceptable while flying on straight lines. However, Figs. 24 to 31 show that the performance significantly worsens at turns when the UAV is located at the outside of the trajectory curve. Although the performance drop is experienced by all MBPs under evaluation, it is important to note that for $\lambda = 10$, the worst network performance at curves is provided by the WT-Distance-Based protocol, while for $\lambda = 15$, the worst network performance is obtained when using the 135Th-Distance-Based MBP. This is a very important observation since it explains the changes in the trajectory performance (i.e., P-RMSE and LU) offered by both protocols when λ increases from 10 to 15 (see Fig. 16 and Fig. 17). Furthermore, note how the trajectory performance is mainly affected by the network performance of the nodes that are located at the formation edges. Thus, the network performance metrics that are traditionally calculated by averaging over all nodes (e.g., Fig. 18 to Fig. 19) within an ad-hoc network deployment (e.g., MANETs and VANETs) cannot be used to fully explain the behavior observed in the trajectory metrics (Fig. 16 and Fig. 17). Therefore, for UAV formation control applications, the results presented in this subsection underline the importance of the trajectory path and time evolution analysis proposed in this paper to evaluate the MBPs suitability for SI dissemination.

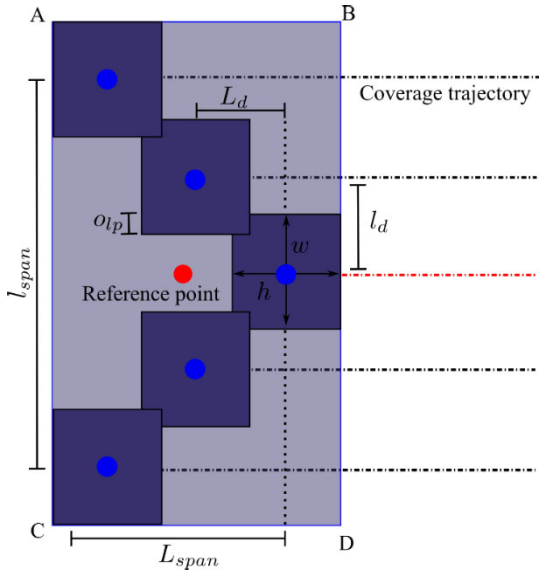

FIGURE 32. Example of a UAV formation for an imaging remote sensing application. $\mathbf{l_{span}}$ and $\mathbf{L_{span}}$ are the lateral and longitudinal spans of the UAV formation, respectively. $\mathbf{l_d}$ and $\mathbf{L_d}$ are the lateral and longitudinal distances of adjacent UAVs in the formation, respectively. w and h are the width and height of the camera (sensor) footprint of each UAV, respectively. The rectangle ABCD defines the area where the UAVs have to simultaneously acquire an image at predefined times.

TABLE 4. Mission scenario parameters.

Parameters	Value
Overlap between neighboring sensing areas, o_{lp}	10 m
Width of neighboring sensing area, w	110 m
Height of neighboring sensing area, h	110 m
Lateral distance, l_d	100 m
Longitudinal distance, L_d	100 m
Height of UAVs flying, H	120 m
Reference trajectory	Sweep trajectory

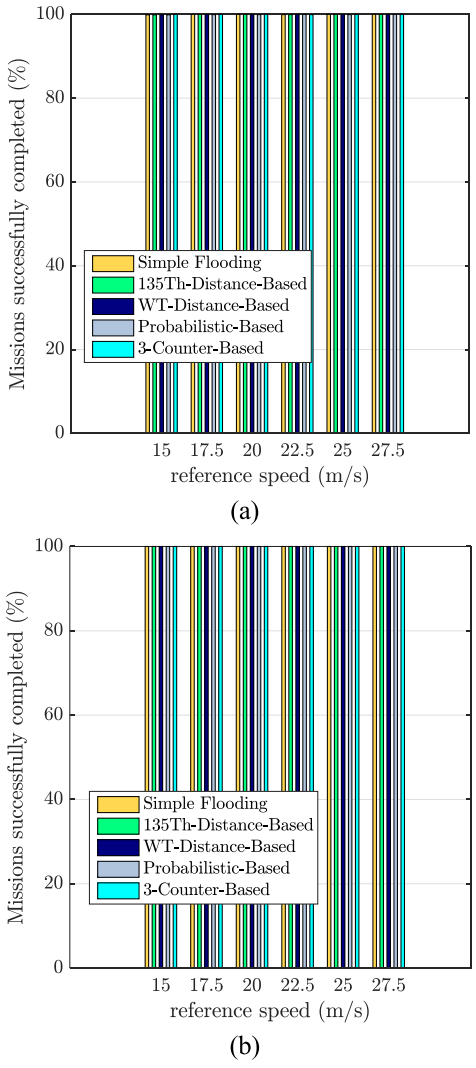

FIGURE 33. Number of missions that were successfully completed using different MBPs for (a) open-delta ($\lambda = 5$) and (b) delta ($\lambda = 6$) formations when varying the reference speed, $\mathbf{v_r}$. The results were obtained with a minimum of 2000 runs to achieve statistical significance.

C. STUDY CASE

As mentioned in the introduction, remote sensing is one of the main applications for multi-UAV systems, e.g., [14], [15], [53], [54], and [56]–[58]. In a remote sensing multi-UAV mission, each UAV captures a series of images (e.g., in the visible light, near-infrared or mid-infrared bands) with a high spatial resolution while flying in formation over a predefined area. Then, the images from all UAVs must be stitched together to obtain the full image of the area of interest and post-processing is performed to extract the desired information, e.g., vegetation indexes. Thus, maintaining a flight formation is crucial in order to be able to cover the desired imaging area with a single flight multi-UAV mission. As such, to further show the relevance of the study performed in this paper, an example of the suitability of the MBPs to disseminate SI messages while performing a multi-UAV imaging remote sensing mission is presented next.

In imaging remote sensing missions, important parameters such as the camera footprint of each UAV or sensing area can be related to flight formation parameters such as the longitudinal and lateral distances between neighbor nodes. Fig. 32 depicts this relationship where the flight formation and overlap parameters (e.g., the overlap between neighboring sensing areas) are shown. The parameters considered for this application example were extracted from existing literature, e.g., [57] and [58], and are shown in Table 4 with their corresponding value.

For each simulation run, a mission is considered to be successful if none of the UAVs in the formation leave the sweep area shown in Fig. 32 during the entire mission. Note that the area itself moves following the reference point during the mission execution. Figs. 33 to 35 show the number of missions successfully completed with the considered MBPs as the reference speed, v_r, increases when UAVs fly in

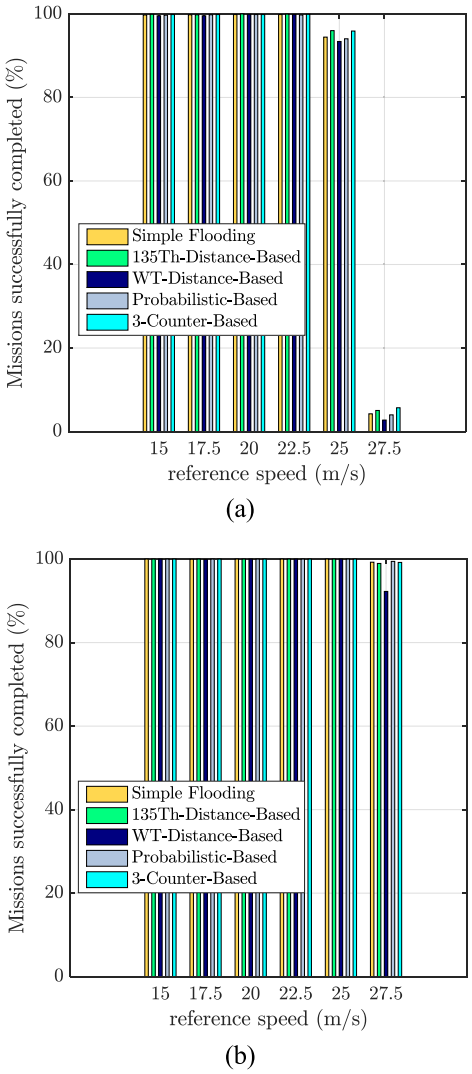

FIGURE 34. Number of missions that were successfully completed using different MBPs for (a) open-delta ($\lambda = 7$) and (b) delta ($\lambda = 10$) formations when varying the reference speed, $\mathbf{v_r}$. The results were obtained with a minimum of 2000 runs to achieve statistical significance.

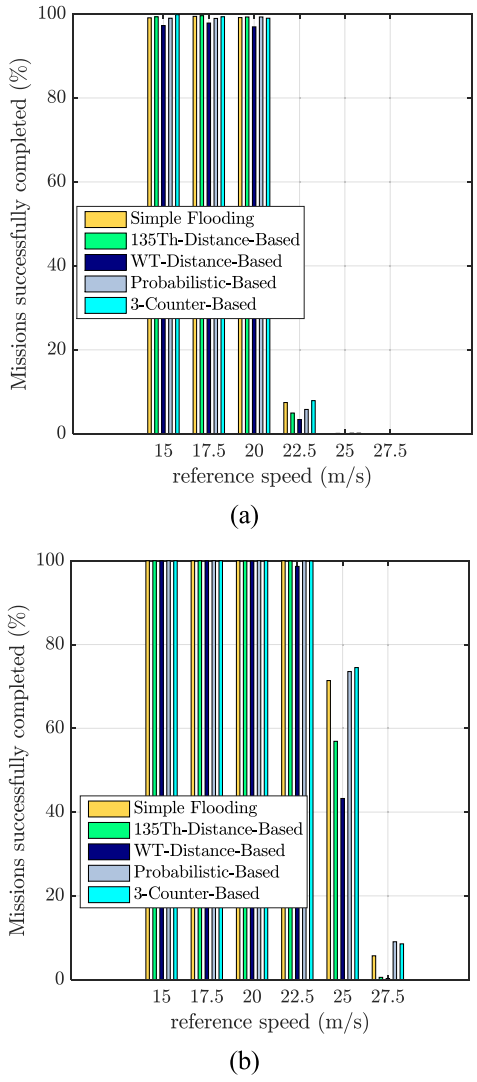

FIGURE 35. Number of missions that were successfully completed using different MBPs for (a) open-delta ($\lambda = 9$) and (b) delta ($\lambda = 15$) formations when varying the reference speed, $\mathbf{v_r}$. The results were obtained with a minimum of 2000 runs to achieve statistical significance.

open-delta and delta formations. The formation size λ ranges from small (Fig. 33) to large (Fig. 35) for each formation type.

By analyzing the results presented in Figs. 33 to 35, the following conclusion can be drawn:

- For missions involving a small number of UAVs (Fig. 33), the selection of the MBP has little impact on the number of successful missions. Moreover, the mission can be executed at high speed ($v_r = 27.5$ m/s) without a negative impact on the mission success.
- For missions involving a medium number of UAVs (Fig. 34), performance degradation starts at $v_r = 25$ m/s for the open-delta formation. In contrast, for the delta formation, a high number of successful missions can be achieved even at high speeds. Thus, for mission planning, it is important to assess the tradeoff between executing the mission with a minimum time (i.e., by using a delta formation with high speed) or with a smaller number of UAVs (i.e., by using an open-delta formation with a low to medium speed).
- For the delta formation with $\lambda = 10$ (Fig. 34(b)), although most MBPs were able to successfully complete a large number of missions for $v_r = 27.5$ m/s, the performance drop that is observed for the WT-Distance-Based protocol discourages its use for this application.
- For missions involving a large number of UAVs (Fig. 35), a significant performance drop is observed at $v_r = 22.5$ m/s for the open-delta formation and at $v_r = 25$ m/s for the delta formation. Nevertheless, in this case, only the delta formation successfully completes 100% of the missions for speeds below $v_r = 25$ m/s.
- For the delta formation with $\lambda = 15$ (Fig. 35(b)), the 3-Counter-Based and Probabilistic-Based MBPs

provided the best performances at high speeds. In contrast, at high speeds, the worst performance is provided by the 135Th-Distance-Based and the WT-Distance-Based protocols. This agrees with the analysis presented in the previous sections.

VII. CONCLUSION

This work studied how the network performance offered by different MBPs that were originally proposed for MANETs and VANETs impacts the effectiveness of distributed UAV formation control to maintain flight formation during a mission execution.

The evaluation results show that even though at low speeds SI dissemination using MBPs is effective in terms of maintaining the UAV formation, as the mission reference speed increases, maintaining formation becomes harder. When comparing the results obtained when using MBPs against ideal SI dissemination, it can be observed that the P-RMSE is higher when an MBP is used. Furthermore, with the ideal SI dissemination, no UAVs are lost. In contrast, some UAVs are lost when using MBPs for SI dissemination, particularly at high speeds. Thus, in actual FANET deployments, it can be stated that the particular MBP used to disseminate SI messages plays a key role in maintaining the formation in distributed UAV formation control.

The obtained results show that factors such as packet losses or delays, that inherently appear in FANETs, affect the suitability of the MBPs for assisting distributed UAV controllers in maintaining a UAV formation. However, to be able to evaluate the performance of the MBPs for distributed UAV formation control applications, a more comprehensive set of metrics should be analyzed. Specifically, the performance of the MBPs was evaluated in terms of the quality of the information that the controller has at each sampling period. Thus, using the PDR is not enough, since the SI age (AvgSIage) at the sampling time is also important. Therefore, the average PDR metric, which is commonly used to assess MBP performance, does not provide enough information to weigh the suitability of MBPs for SI dissemination in distributed UAV formation control applications. This is highlighted by the trajectory metrics (P-RMSE and LU) obtained for the delta formation at high speeds when using the 135Th-Distance-Based MBP, which were worse than those obtained when using Simple Flooding, even though 135Th-Distance-Based exhibits a higher average PDR.

To further analyze the performance of the MBPs, the costs of each protocol to achieve a particular PDR were evaluated using the average collision ratio (CR), and the average packet rebroadcasts canceled (PRC) metrics. The use of these average metrics is proposed in this paper to perform an initial assessment of the suitability of the MBPs for SI dissemination. In this sense, for the delta formation and high speeds, it can be observed that although a high PRC adversely affects the trajectory performance (e.g., WT-Distance-Based), the best trajectory performance was not obtained when the PRC was equal to zero, as in the case of Simple Flooding. In fact, for this scenario the best performance was provided by the Probabilistic-Based and 3-Counter-Based MBPs, which exhibited relatively low PRCs and high PDRs. Therefore, it can be stated that there is a need to propose new MBPs that are specifically designed for SI dissemination and consider these issues.

Using average network metrics (which is commonly done for MANETs and VANETs) is a good starting point for the evaluation of MBPs. However, when they are used to evaluate the performance of the MBPs for SI dissemination in distributed UAV formation control applications, average network metrics do not fully explain the results observed for the trajectory metrics. Thus, in this work, the use of moving average network metrics is proposed to gain more insight into the performance of the MBPs for this kind of application. By using moving average metrics, it was found that the performance of most MBPs significantly worsens when the formation makes a turn. This is particularly acute for UAVs that are located at edges of the formation, which receive SI messages through multiple hops. Thus, by performing moving average analysis, the key zones of the flight formation where the relevance of the information quality (e.g., AvgSIage) is higher can be detected. This further highlights the need to design new MBP strategies that are focused on SI dissemination for distributed UAV formation control.

Finally, note that except for Simple Flooding, all protocols under evaluation include mechanisms that cancel packet retransmissions when a certain criterion is fulfilled. Therefore, in addition to collisions and propagation phenomena, a distant node might not receive an SI packet because of a rebroadcast cancellation. Thus, the results and analysis that are provided in this paper show that more than simply selecting any MBP to disseminate SI messages in FANETs, it is necessary to design a protocol that can adapt to the conditions of the target scenario. Future work includes developing an adaptive MBP based on attributes such as the curvature and reference speed, which can be calculated on the fly during the mission. Additionally, future work will include evaluating the adaptive MBP for different adverse conditions such as wind disturbance.

REFERENCES

[1] S. Hayat, E. Yanmaz, and R. Muzaffar, "Survey on unmanned aerial vehicle networks for civil applications: A communications viewpoint," *IEEE Commun. Surveys Tuts.*, vol. 18, no. 4, pp. 2624–2661, 4th Quart., 2016.

[2] J. George, P. B. Sujit, and J. B. Sousa, "Search strategies for multiple UAV search and destroy missions," *J. Intell. Robot. Syst.*, vol. 61, nos. 1–4, pp. 355–367, 2011.

[3] M. Hassanalian and A. Abdelkefi, "Classifications, applications, and design challenges of drones: A review," *Progr. Aerosp. Sci.*, vol. 91, pp. 99–131, May 2017.

[4] V. Sharma, H.-C. Chen, and R. Kumar, "Driver behaviour detection and vehicle rating using multi-UAV coordinated vehicular networks," *J. Comput. Syst. Sci.*, vol. 86, pp. 3–32, Jun. 2017.

[5] G. Cai, J. Dias, and L. Seneviratne, "A survey of small-scale unmanned aerial vehicles: Recent advances and future development trends," *Unmanned Syst.*, vol. 2, no. 2, pp. 175–199, 2014.

[6] O. K. Sahingoz, "Networking models in flying ad-hoc networks (FANETs): Concepts and challenges," *J. Intell. Robot. Syst.*, vol. 74, nos. 1–2, pp. 513–527, 2014.

[7] I. Bekmezci, O. K. Sahingoz, and Ş. Temel, "Flying ad-hoc networks (FANETs): A survey," *Ad Hoc Netw.*, vol. 11, no. 3, pp. 1254–1270, 2013.
[8] T. Andre, K. A. Hummel, A. P. Schoellig, E. Yanmaz, M. Asadpour, C. Bettstetter, P. Grippa, H. Hellwagner, S. Sand, and S. Zhang, "Application-driven design of aerial communication networks," *IEEE Commun. Mag.*, vol. 52, no. 5, pp. 129–137, May 2014.
[9] I. Vidal, F. Valera, M. A. Diaz, and M. Bagnulo, "Design and practical deployment of a network-centric remotely piloted aircraft system," *IEEE Commun. Mag.*, vol. 52, no. 10, pp. 22–29, Oct. 2014.
[10] M. Simunek, F. P. Fontán, and P. Pechac, "The UAV low elevation propagation channel in urban areas: Statistical analysis and time-series generator," *IEEE Trans. Antennas Propag.*, vol. 61, no. 7, pp. 3850–3858, Jul. 2013.
[11] Y. Zou, P. R. Pagilla, and R. T. Ratliff, "Distributed formation flight control using constraint forces," *J. Guid. Control. Dyn.*, vol. 32, no. 1, pp. 112–120, 2009.
[12] B. D. O. Anderson, B. Fidan, C. Yu, and D. Walle, "UAV formation control: Theory and application," in *Recent Advances in Learning and Control* (Lecture Notes in Control and Information Sciences), vol. 371. London, U.K.: Springer, 2008, pp. 15–33.
[13] R. Kristiansen, E. Oland, and D. Narayanachar, "Operational concepts in UAV formation monitoring of industrial emissions," in *Proc. 3rd IEEE Int. Conf. Cogn. Infocommun. (CogInfoCom)*, Dec. 2012, pp. 339–344.
[14] C. Ju and H. Son, "Multiple UAV systems for agricultural applications: Control, implementation, and evaluation," *Electronics*, vol. 7, no. 9, p. 162, Aug. 2018.
[15] M. Quaritsch, K. Kruggl, D. Wischounig-Strucl, S. Bhattacharya, M. Shah, and B. Rinner, "Networked UAVs as aerial sensor network for disaster management applications," *e & i Elektrotechnik und Informationstechnik*, vol. 127, no. 3, pp. 56–63, 2010.
[16] Y. Gu, B. Seanor, G. Campa, M. R. Napolitano, L. Rowe, S. Gururajan, and S. Wan, "Design and flight testing evaluation of formation control laws," *IEEE Trans. Control Syst. Technol.*, vol. 14, no. 6, pp. 1105–1112, Nov. 2006.
[17] X. Wang, Z. Zeng, and Y. Cong, "Multi-agent distributed coordination control: Developments and directions via graph viewpoint," *Neurocomputing*, vol. 199, pp. 204–218, Jul. 2016.
[18] Y. Cao, W. Yu, W. Ren, and G. Chen, "An overview of recent progress in the study of distributed multi-agent coordination," *IEEE Trans. Ind. Informat.*, vol. 9, no. 1, pp. 427–438, Feb. 2013.
[19] I. Bekmezci, I. Sen, and E. Erkalkan, "Flying ad hoc networks (FANET) test bed implementation," in *Proc. 7th Int. Conf. Recent Adv. Space Technol. (RAST)*, Jun. 2015, pp. 665–668.
[20] Y. Zeng, R. Zhang, and T. J. Lim, "Wireless communications with unmanned aerial vehicles: Opportunities and challenges," *IEEE Commun. Mag.*, vol. 54, no. 5, pp. 36–42, May 2016.
[21] L. Gupta, R. Jain, and G. Vaszkun, "Survey of important issues in UAV communication networks," *IEEE Commun. Surveys Tuts.*, vol. 18, no. 2, pp. 1123–1152, 2nd Quart., 2016.
[22] S. Panichpapiboon and W. Pattara-atikom, "A review of information dissemination protocols for vehicular ad hoc networks," *IEEE Commun. Surveys Tuts.*, vol. 14, no. 3, pp. 784–798, 3rd Quart., 2012.
[23] A. Bujari, C. T. Calafate, J.-C. Cano, P. Manzoni, C. E. Palazzi, and D. Ronzani, "Flying ad-hoc network application scenarios and mobility models," *Int. J. Distrib. Sens. Netw.*, vol. 13, no. 10, 2017, Art. no. 1550147717738192.
[24] O. S. Oubbati, A. Lakas, F. Zhou, M. Günes, and M. B. Yagoubi, "A survey on position-based routing protocols for flying ad hoc networks (FANETs)," *Veh. Commun.*, vol. 10, pp. 29–56, Oct. 2017.
[25] Y. Ke, J. Wang, J. Wang, and Y. Ke, "Nonlinear formation control of small fixed-wing UAVs with velocity and heading rate constraints," in *Proc. IEEE Int. Conf. Mechatronics Autom. (ICMA)*, Aug. 2018, pp. 1275–1280.
[26] M. Turpin, N. Michael, and V. Kumar, "Trajectory design and control for aggressive formation flight with quadrotors," *Auto. Robots*, vol. 33, nos. 1–2, pp. 143–156, 2012.
[27] C. Park, N. Cho, K. Lee, and Y. Kim, "Formation flight of multiple UAVs via onboard sensor information sharing," *Sensors*, vol. 15, no. 7, pp. 17397–17419, 2015.
[28] M. Lei, S.-L. Zhou, X.-X. Yang, and G.-Y. Yin, "Complex formation control of large-scale intelligent autonomous vehicles," *Math. Problems Eng.*, vol. 2012, Oct. 2012, Art. no. 241916.
[29] Y. Ben-Asher, S. Feldman, P. Gurfil, and M. Feldman, "Distributed decision and control for cooperative UAVs using ad hoc communication," *IEEE Trans. Control Syst. Technol.*, vol. 16, no. 3, pp. 511–516, May 2008.
[30] Y. Kuriki and T. Namerikawa, "Formation control with collision avoidance for a multi-UAV system using decentralized MPC and consensus-based control," *J. Control. Meas. Syst. Integr.*, vol. 8, no. 4, pp. 285–294, 2015.
[31] M. Ille and T. Namerikawa, "Collision avoidance between multi-UAV-systems considering formation control using MPC," in *Proc. IEEE Int. Conf. Adv. Intell. Mechatronics (AIM)*, Jul. 2017, pp. 651–656.
[32] T. Chevet, C. Vlad, C. S. Maniu, and Y. Zhang, "Decentralized MPC for UAVs formation deployment and reconfiguration with multiple outgoing agents," *J. Intell. Robot. Syst.*, pp. 1–16, Apr. 2019. doi: 10.1007/s10846-019-01025-x.
[33] A. Abdessameud, I. G. Polushin, and A. Tayebi, "Motion coordination of thrust-propelled underactuated vehicles with intermittent and delayed communications," *Syst. Control Lett.*, vol. 79, pp. 15–22, May 2015.
[34] Z. Chao, S.-L. Zhou, L. Ming, and W.-G. Zhang, "UAV formation flight based on nonlinear model predictive control," *Math. Problems Eng.*, vol. 2012, Oct. 2011, Art. no. 261367.
[35] D. Lee, S.-W. Chang, and S.-S. Lee, "Analysis and design on efficient message relay methods in VANET," *Multimedia Tools Appl.*, vol. 74, no. 16, pp. 6331–6340, 2014.
[36] Y.-C. Tseng, S.-Y. Ni, Y.-S. Chen, and J.-P. Sheu, "The broadcast storm problem in a mobile ad hoc network," *Wireless Netw.*, vol. 8, nos. 2–3, pp. 153–167, 2002.
[37] N. Wisitpongphan, O. K. Tonguz, J. S. Parikh, P. Mudalige, F. Bai, and V. Sadekar, "Broadcast storm mitigation techniques in vehicular ad hoc networks," *IEEE Wireless Commun.*, vol. 14, no. 6, pp. 84–94, Dec. 2007.
[38] A. Richards and J. How, "Decentralized model predictive control of cooperating UAVs," in *Proc. IEEE Conf. Decis. Control*, vol. 4, Dec. 2004, pp. 4286–4291.
[39] J. Shin and H. J. Kim, "Nonlinear model predictive formation flight," *IEEE Trans. Syst., Man, Cybern. A, Syst. Hum.*, vol. 39, no. 5, pp. 1116–1125, Sep. 2009.
[40] R. de Melo Pires, S. Z. Arnosti, A. S. R. Pinto, and K. R. L. J. C. Branco, "Experimenting broadcast storm mitigation techniques in FANETs," in *Proc. 49th Hawaii Int. Conf. Syst. Sci. (HICSS)*, Jan. 2016, pp. 5868–5877.
[41] V. Sharma, R. Kumar, and N. Rathore, "Topological broadcasting using parameter sensitivity-based logical proximity graphs in coordinated ground-flying ad hoc networks," *J. Wireless Mobile Netw., Ubiquitous Comput. Dependable Appl.*, vol. 6, no. 3, pp. 54–72, 2015.
[42] A. Bujari, C. E. Palazzi, and D. Ronzani, "A comparison of stateless position-based packet routing algorithms for FANETs," *IEEE Trans. Mobile Comput.*, vol. 17, no. 11, pp. 2468–2482, Nov. 2018.
[43] J. Chen, D. Sun, J. Yang, and H. Chen, "Leader-follower formation control of multiple non-holonomic mobile robots incorporating a receding-horizon scheme," *Int. J. Robot. Res.*, vol. 29, no. 6, pp. 727–747, 2010.
[44] Y. Zhang and H. Mehrjerdi, "A survey on multiple unmanned vehicles formation control and coordination: Normal and fault situations," in *Proc. Int. Conf. Unmanned Aircr. Syst. (ICUAS)*, May 2013, pp. 1087–1096.
[45] K. D. Do and J. Pan, "Nonlinear formation control of unicycle-type mobile robots," *Robot. Auton. Syst.*, vol. 55, no. 3, pp. 191–204, 2007.
[46] J. R. T. Lawton, R. W. Beard, and B. J. Young, "A decentralized approach to formation maneuvers," *IEEE Trans. Robot. Autom.*, vol. 19, no. 6, pp. 993–941, 2003.
[47] W. Ren and E. Atkins, "Nonlinear trajectory tracking for fixed wing UAVs via backstepping and parameter adaptation," in *Proc. AIAA Guid. Navigation Control Conf. Exhib.*, Nov. 2005, pp. 1–11.
[48] *INET Framework for OMNeT++ Manual*, OMNeT++, Budapest, Hungary, 2012.
[49] B. Houska, H. J. Ferreau, M. Vukov, and R. Quirynen, "ACADO toolkit users manual," OPTEC, Leuven, Belgium, Tech. Rep. 1.2.1, 2014.
[50] N. Goddemeier and C. Wietfeld, "Investigation of air-to-air channel characteristics and a UAV specific extension to the rice model," in *Proc. IEEE Globecom Workshops*, Dec. 2015, pp. 1–5.
[51] *IEEE Standard for Information Technology–Local and Metropolitan Area Networks–Specific Requirements—Part 11: Wireless LAN Medium Access Control (MAC) and Physical Layer (PHY) Specifications Amendment 6: Wireless Access in Vehicular Environments*, IEEE Standard 80211p-2010, IEEE 80211-2007, IEEE 80211k-2008, IEEE 80211r-2008, IEEE 80211y-2008, IEEE 80211n-2009, IEEE 80211w-2009, 2010, pp. 1–51.
[52] I. Maza and A. Ollero, "Multiple UAV cooperative searching operation using polygon area decomposition and efficient coverage algorithms," in *Distributed Autonomous Robotic Systems 6*. Tokyo, Japan: Springer, 2007, pp. 221–230.

[53] G. S. C. Avellar, G. A. S. Pereira, L. C. A. Pimenta, and P. Iscold, "Multi-UAV routing for area coverage and remote sensing with minimum time," *Sensors*, vol. 15, no. 11, pp. 27783–27803, Nov. 2015.
[54] S. S. Mansouri, C. Kanellakis, G. Georgoulas, D. Kominiak, T. Gustafsson, and G. Nikolakopoulos, "2D visual area coverage and path planning coupled with camera footprints," *Control Eng. Pract.*, vol. 75, pp. 1–16, Jun. 2018.
[55] T. S. Rappaport, *Wireless Communications: Principles and Practice*, 2nd ed. Upper Saddle River, NJ, USA: Prentice-Hall, 2002.
[56] F. Balampanis, I. Maza, and A. Ollero, "Coastal areas division and coverage with multiple UAVs for remote sensing," *Sensors*, vol. 17, no. 4, p. 808, 2017.
[57] H. Chao, M. Baumann, A. Jensen, Y. Chen, Y. Cao, W. Ren, and M. McKee, "Band-reconfigurable multi-UAV-based cooperative remote sensing for real-time water management and distributed irrigation control," *IFAC Proc. Vols.*, vol. 41, no. 2, pp. 11744–11749, 2008.
[58] M. Erdelj, M. Król, and E. Natalizio, "Wireless sensor networks and multi-UAV systems for natural disaster management," *Comput. Netw.*, vol. 124, pp. 72–86, Sep. 2017.

E. GIOVANNI CABRAL-PACHECO received the B.S. degree in electronics and communications from the Autonomous University of Zacatecas, Mexico, in 2011, and the M.Sc. degree in electronics and telecommunication from the CICESE Research Center, Ensenada, Mexico, in 2014, where he is currently pursuing the Ph.D. degree in electronics and telecommunications. His research interests include ad-hoc networks, vehicular ad-hoc networks, flying ad-hoc networks, the IoT, wireless sensor networks, machine learning, digital signal processing, among others.

SALVADOR VILLARREAL-REYES received the B.Sc. (Eng.) degree in electronics engineering from the Durango Institute of Technology, Durango, Mexico, the M.Sc. degree in electronics engineering (telecommunications) from the Monterrey Institute of Technology and Higher Education, Monterrey, Mexico, in 1998 and 2001, respectively, and the Ph.D. degree in electrical and electronics engineering from Loughborough University, U.K., in 2007. He is currently a Titular Researcher with the CICESE Research Center in Ensenada, Mexico. His research interests include ad-hoc networks, vehicular ad-hoc networks, flying ad-hoc networks, the IoT, Internet of medical things (m-IoT), e-Health systems, m-Health systems, wireless sensor networks, digital signal processing, embedded systems, among others.

ALEJANDRO GALAVIZ-MOSQUEDA received the M.Sc. degree in computer science from the University of Colima, México, in 2006, and the Ph.D. degree from the CICESE Research Center, Mexico, in 2013. He is currently a Researcher with the CONACYT-CICESE Unidad Monterrey, Mexico. His main research interests include mobile and wireless networks for intelligent transport systems and mHealth.

SERGIO VILLARREAL-REYES received the M.Sc. degree in information technologies from the Monterrey Institute of Technology and Higher Education, Monterrey, Mexico, in 2007, where he is currently pursuing the Ph.D. degree. His research interests include embedded systems, wireless networks, routing protocols, vehicular ad-hoc network software engineering, databases systems, among others.

RAUL RIVERA-RODRIGUEZ received the B.Sc. (Eng.) degree in electronics engineering from the Sonora Institute of Technology, Sonora, Mexico, the M.Sc. degree in electronics and telecommunications from the CICESE Research Center, Ensenada, Mexico, in 1994 and 1997, respectively, and the Ph.D. from the Autonomous University of Baja California, Baja California, Mexico, in 2010. He contributed to deploy the National Research for Education Network Infrastructure in Mexico as the President of the Network Committee of CUDI. He is currently the Director of the Telematics Division, CICESE Research Center, Ensenada. His research interests include network management systems, QoS in IP networks, signal processing for wireless communications, multimedia communications, communication networks, cross-layer design, and coding theory.

ALDO E. PEREZ-RAMOS received the B.Sc. (Eng.) degree in electronics engineering from the Oaxaca Institute of Technology, Oaxaca, Mexico, and the M.Sc. and Ph.D. degrees in electronics and telecommunications from the CICESE Research Center in Ensenada, Mexico, in 2008 and 2016, respectively. He is currently a Postdoctoral Researcher with CICESE. His main research interests include wireless personal area networks, wireless sensor networks, radio over fiber architectures, embedded systems, m-health systems, among others.